Research Article

Glacial–interglacial cycles in the south-central and southeastern Pyrenees since ~180 ka (NE Spain–Andorra–S France)

Valenti Turu[a,b,c,d*] ![ORCID], Jose Luís Peña-Monné[e], Pedro P. Cunha[f], Guy Jalut[a], Jan-Pieter Buylaert[g], Andrew S. Murray[h], David Bridgland[i], Mads Faurschou-Knudsen[j], Marc Oliva[d], Rosa M. Carrasco[c], Xavier Ros[a], Laia Turu-Font[k] ![ORCID] and Josep Ventura Roca[a,c,d]

[a]Marcel Chevalier Earth Science Foundation, Andorra la Vella, Principat d'Andorra, AD500, Andorra; [b]Departament de Dinàmica de la Terra i l'Oceà, Facultat de Ciències de la Terra, Universidad de Barcelona, 08028 Barcelona, Spain; [c]Department of Environmental Sciences, Castilla-La Mancha University, 45004 Toledo Spain; [d]ANTALP (Antarctic, Arctic and Alpine Environments), Department of Geography, Barcelona University, 08001 Barcelona, Spain; [e]Departamento de Geografía y Ordenacion del Territorio and IUCA, Universidad de Zaragoza, 50009 Zaragoza, Spain; [f]University of Coimbra, MARE—Marine and Environmental Sciences Centre / ARNET, Department of Earth Sciences, 3000-195 Coimbra, Portugal; [g]Department of Physics, Technical University of Denmark, DK-2800 Risø Campus, Denmark; [h]Nordic Laboratory for Luminescence Dating, Aarhus University, DK-8000 Aarhus, Denmark; [i]Department of Geography, Durham University, Stackton Road, DH1 3LE England, United Kingdom; [j]Department of Geoscience, Aarhus University, DK-8000 Aarhus, Denmark and [k]Departament de Ciències de l'Antiguitat i l'Edat Mitjana, Universitat Autònoma de Barcelona, 08193 Bellaterra, Spain

Abstract

This study uses luminescence and ^{14}C accelerator mass spectrometry procedures to date relevant glaciofluvial and glacial deposits from the south-central and southeastern Pyrenees (Andorra–France–Spain). We distinguish two types of end-moraine complexes: (1) those in which at least a far-flung moraine exists beyond a frequently nested end-moraine complex (the most common) and (2) those in which a close-nested end moraine encompasses at least two glacial cycles. Both types formed within six distinctive glacial intervals: (1) A penultimate glacial cycle during Marine Oxygen Isotope Stage (MIS) 6 and older glaciofluvial terraces occurred beyond the range of the luminescence dating method. (2) An early glacial advance in MIS 5d ($\sim$97 $-15/+19$ ka) was followed by glacial retreat during MIS 5c (< 91 $\pm$ 9 ka). (3) The last maximum ice extent (LMIE) was in early MIS 4 ($\sim$74 $\pm$ 4.5 ka). (4) Unexpectedly, glaciers thinned during the second half of MIS 3 ($\sim$39 $-6/+11$ ka). (5) During the MIS 3–2 transition, glaciers subsequently fluctuated behind the LMIE limits. (6) The global last glacial maximum (LGM) started as early as $\sim$26.6 $\pm$ 0.365 ka b2k, and the corresponding end moraines were built behind the LMIE limits or merged with it, forming close-nested moraines.

Keywords: End moraines, Penultimate glacial cycle, Last glacial cycle, SW Europe, Luminescence dating methods

INTRODUCTION

The glacial footprint in the Mediterranean region is restricted to mountain ranges, where later ones overprint earlier glacial cycles. The most prominent glaciation in the Mediterranean region was before 350 ka (Giraudi and Giaccio, 2017), conditioning the sediment storage of rivers (Woodward et al., 2008). A glacial cycle is indicated in between the Marine Oxygen Isotope Stage (MIS) 7 interglacial and MIS 12 (Woodward et al., 2008; Hughes et al., 2011), matching with the oldest dated outwash deposits on both sides of the Pyrenean mountain belt (Lewis et al., 2009; Delmas et al., 2015), which are attributed to MIS 8. However, evidence

of old glaciations in Iberia is sparse (Turu and Peña-Monné, 2006; Lewis et al., 2009; Jalut et al., 2010; García-Ruiz et al., 2013; Villa et al., 2013; Delmas et al., 2021a). Nevertheless, the penultimate glaciation (MIS 6) has been identified in most of the Iberian ranges (Vidal-Romaní et al., 1999, 2015; Turu and Peña-Monné, 2006; García-Ruiz et al., 2013; Rodríguez-Rodríguez et al., 2016; Vieira et al., 2021; Fernandes et al., 2021) and coincided with a significant episode of fluvial aggradation (Turu and Peña-Monné, 2006; Lewis et al., 2009; Stange et al., 2013, 2014; Delmas et al., 2015).

Regarding the last glacial cycle (LGC), glacial expansion started as early as MIS 5d in the Mediterranean region (Hughes et al., 2010). In Iberia, the local last glacial maximum would be between 23 and 17.5 ka (Roucoux et al., 2005; Oliva et al., 2019). However, in the Pyrenees, the last maximum ice extent (LMIE) predates the last glacial maximum (LGM) of the northern ice sheets (Mardones and Jalut, 1983; Vilaplana, 1983a; Jalut et al., 1992, 2010; Delmas et al., 2021a and references therein). Based on rapid

cooling and precipitation levels similar to those of MIS 2, it has been suggested that the LMIE probably coincided with MIS 4 (Clapperton, 1997; Doughty et al., 2021). In addition, there is fragmentary evidence of an earlier maximum ice extent (MIE) (Bakalowicz et al., 1984; Hetu et al., 1992; Turu and Peña-Monné, 2006; Turu et al., 2007; Ventura and Turu, 2022). At the end of MIS 4, ice recession matched with the increase of summer daily insolation at 65°N until interstadial GI-17 (Martrat et al., 2004). During Heinrich event H6 (61–59 ka), steppe pollen increased, suggesting an arid climate (Roucoux et al., 2005). However, insolation slightly diminished until interstadial GI-7 ($\approx$35 ka) is more pronounced, declining until stadial GS-3 ($\approx$27 ka), corresponding with a phase of significant glacial readvances in the Pyrenees (Turu, 2018). To gain a better understanding of the palaeoenvironmental conditions of the LGC, causes of the LMIE/LGM dephasing and the chronological position of the MIE, some authors have investigated relevant glaciolacustrine sequences in the Pyrenees (Jalut et al., 1992, 2010; González-Sampériz et al., 2006; Turu and Bordonau, 2013; Turu et al., 2017; Sancho et al., 2018), sediments from glacially overdeepened valleys (Bordonau, 1992; Turu, 2000; Turu et al., 2007; Salazar-Rincón et al., 2013), lacustrine foreland sequences (Pérez-Obiol and Julià, 1994; Höbig et al., 2012; González-Sampériz et al., 2017), or fluvial terraces (Peña-Monné et al., 2011; Stange et al., 2014; Delmas et al., 2015) or have focused on lateral glacial (kame-type deposits) and terminal complexes (end moraines and glaciofluvial deposits) (Turu and Peña-Monné, 2006; Lewis et al., 2009, 2017; Pallàs et al., 2010; Delmas et al., 2011; Bartolomé et al., 2021; Fernandes et al., 2021; among others).

Asymmetries arise when comparing both sides of the mountain range. On the one hand, we have the example of the SW Pyrenees, in which the MIE is from the penultimate glaciation (Lewis et al., 2009; García-Ruiz et al., 2013), but this is not the case in the SE Pyrenees, where glacial extent during the penultimate glacial cycle (PGC) was less than during the LMIE (Turu et al., 2007; Ventura and Turu, 2022). On the other hand, evidence from the LGM is somewhat elusive in the SW Pyrenees (García-Ruíz et al., 2003, 2013; Lewis et al., 2009; Bartolomé et al., 2021). Aridity (Höbig et al., 2012; Allard et al., 2021) and moisture variations (Jalut et al., 2010; Delmas et al., 2015; Turu, 2018) seem to have provided strong gradients between the Atlantic and the Mediterranean and exerted a significant influence on glacial extent across the Pyrenees. A W–E moisture gradient during the Holocene has been demonstrated in Iberia (Liu et al., 2021) and during the last termination period in the Iberian Central System mountain range (Turu et al., 2018, 2021). A similar NW–SE gradient is expected to have existed across the Pyrenean range during glaciations.

Before attempting any discussion comparing the existing data identifying glacial cycles or phases in the Pyrenees, some additional chronological data from relevant sites is needed. To do this task, we chose end moraines and terminal complexes within glacial valleys from the south-central and southeastern Pyrenees, especially far-flung moraines (Anderson et al., 2012) and nested moraines (Kirkbride and Winkler, 2012).

GEOMORPHOLOGICAL SETTINGS AND GLACIAL ANTECEDENTS

The Segre River tributary catchments are located on the southern slope of the French–Spanish–Andorran Pyrenees, draining to the Ebro basin and thus to the Mediterranean Sea (Fig. 1). From east to west, the Segre tributaries are the Valira, Noguera Pallaresa, Noguera Ribagorçana, and Cinca Rivers. Most of the southern Pyrenean glacial valleys are U-shaped, flanked by lateral moraines, kame-type deposits, and former ice-dammed valleys. From west to east, the highest peaks in the studied area are the Pic de Margalida (3251 m) in the Noguera Ribagorçana, followed by Pica d'Estats (3143 m) in the Noguera Pallaresa on the France–Spain border, the Comapedrosa (2942 m) in the northwest of Andorra, and the Carlit (2921 m) in the French Cerdagne (Fig. 1). Most of the end-moraine complexes from the southeastern and south-central Pyrenees did not reach the foreland foothills, with only the Valira and Querol palaeoglaciers having reached the intramountain grabens of the Urgellet and Cerdagne, respectively (Calvet, 1998; Turu et al., 2007).

The Upper Noguera Ribagorçana valley

This valley is located on the westernmost side of the studied area (Fig. 1, sector 1). Geologically speaking, three rock types are present in this valley, distributed following a W–E trend (Mey, 1965): late Variscan crystalline rocks (granites) on the northern part of the valley (north from the Baserca reservoir; Fig. 2), Mesozoic sedimentary rocks southward from the confluence of the Baliera River and the Noguera Ribagorçana River (south Vilaller; Fig. 2), and finally, Palaeozoic low-grade metamorphic rocks in between the two previous lithological areas. Geomorphologically speaking, the valley harbours thick lateral moraines and kame deposits well suited to study glacial evolution.

The upper Noguera Ribagorçana was the first glacial valley from the southern slope of the Pyrenees to be dated, specifically in the Llauset (Fig. 2) glaciolacustrine deposits (Vilaplana, 1983a, 1983b; Montserrat-Martí, 1985) when the lake water level was artificially raised to become the reservoir for a pumped-storage hydroelectric power plant. In the same area, the former Llestui ice-dammed glaciolacustrine complex was the next to be dated (Vilaplana et al., 1989; Vilaplana and Bordonau 1989; Bordonau et al., 1993) along with the Seminari de Vilaller (Fig. 2) overdeepened trough (Bordonau, 1992). Half a kilometre northward from Sant Mamés (Fig. 2), a terminal-moraine complex was identified at Seminari de Vilaller (Vilaplana, 1983a, 1983b; Bordonau et al., 1989; Bordonau, 1992; Pallàs et al., 2006). Nearby, erratic boulders at Tinabre (Fig. 2) have produced the oldest [10]Be cosmic ray exposure (CRE) ages in the valley (Pallas et al., 2006). No end-moraine exposures south of Vilaller are currently known. However, the remains of glaciofluvial and kame deposits help us to reconstruct the LMIE glacial front in Pont de Suert (Fig. 2).

The upper Noguera Pallaresa valley

Surrounded mainly by low-grade metamorphic rocks (Zandvliet, 1960), the former Noguera Pallaresa glacier benefitted from the contribution of the former Garonne glacier coming from the NW side of the valley (the Beret and Bonaigua pass; Fig. 1) and produced the most extensive glacial tongue (63 km) in the southern Pyrenees (Ventura and Turu, 2022). The terminal-moraine complex from the LGC was identified $\sim$2 km upstream from Sort (Fig. 1, sector 2) at 748 m above sea level (m asl; Bastida de Sort; Furdada, 1988; Ventura and Turu, 2022). Unfortunately, no other end moraine has been identified from the Noguera Pallaresa glacier. However, a thick glaciofluvial terrace is located in Sort (Fig. 1).
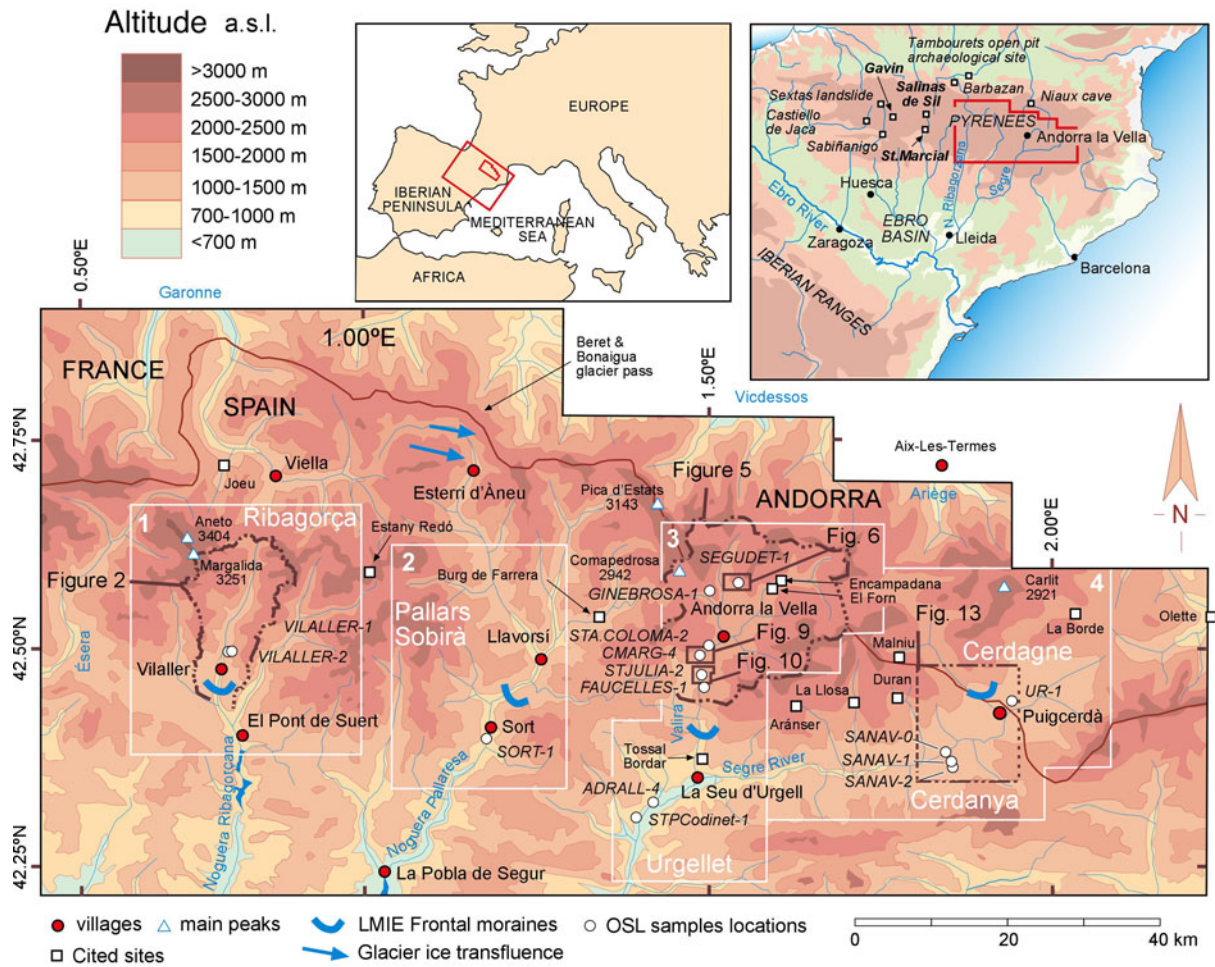
Figure 1. Study area location. Sector 1: Upper Noguera Ribagorzana (Ribagorça region); sector 2: Upper Noguera Pallaresa (Pallars Sobirà region); sector 3: Valira and Segre valleys (Andorra and Urgellet regions); sector 4: Cerdanya (Cerdagne) and Upper Segre valleys. Detailed figures and optically stimulated luminescence (OSL) samples are included in the map. It also contains the glacial ice transfluences and last maximum ice extent (LMIE) frontal moraines.

The Valira valleys

The main Valira glacier (Fig. 1, sector 3) was formed by the confluence of two tributaries, the former Valira del Nord glacier and the Valira d'Orient glacier (Fig. 3). Both tributaries flowed over metamorphic rocks grading from slates to gneiss. However, the floors of these valleys are in granite bedrock (Zwart, 1979). The resulting ice tongue (Fig. 3) extended from Escaldes-Engordany (1050 m) to beyond Sant Julià de Lòria (900 m) (Turu et al., 2007) and formed several terminal-moraine complexes (Cal Tolse, Sant Julià de Lòria, La Margineda, and Santa Coloma; Fig. 3), mainly related to readvances within general deglaciation (Turu et al., 2007, 2017).

The southernmost deposits are the Cal Tolse terminal-moraine complex (Turu, 1994), exposed in an ancient quarry located +85 m above the riverbed (m arb), which exploited aggregates from glaciofluvial deposits southward from Sant Julià de Lòria (Fig. 3). This area was exposed by the triggering of a landslide in 2018 (Luzi et al., 2021), allowing identification of a supraglacial till that is partially eroded and overlain by glaciofluvial deposits.

The subsequent deposits are in Sant Julià de Lòria (Fig. 3), where Prat (1980) identified erratic boulders on the eastern Valira riverbank. Later, building works allowed a better view of the terminal complex (Jalut and Turu, 2008).

Upstream from Sant Julià de Lòria is the La Margineda terminal complex, long established as an end moraine from the Valira glacier (Panzer, 1926; Nussbaum, 1934; Llobet, 1947). Here colluvium overlies glaciofluvial deposits located at 905 m (45 m arb; Turu, 1994); however, only occasional exposures of a supraglacial till have been seen during building excavations. Weathered granite boulders were identified at 980 m and attributed to an old moraine (the Llumaneres moraine from Turu and Peña-Monné, 2006). Nevertheless, a large outcrop to the south of La Margineda allows the identification of a fresher end moraine.

In Santa Coloma (Fig. 3), an open pit cut into a fluvial terrace +15 m arb by an ancient quarry provided an opportunity for Nussbaum (1956) to recognize a moraine from the Valira glacier when it had a length of 29 km (Chevalier, 1906, 1907). Upstream from Santa Coloma many other retreat moraines have been recognized (Bladé, 1875; Penck, 1884; Turu et al., 2017 and references therein), but these were not revisited in this study.

The best-preserved glacial deposits studied in Andorra are from ice-dammed and kame-terrace complexes, as in association with the La Massana palaeolake (Serrat and Vilaplana, 1979), where glaciolacustrine deposits are common (Serrat et al., 1983; Vilaplana, 1984, 1985; Turu, 2018 and references therein). We revisited key exposures, such as the Ginebrosa and Segudet
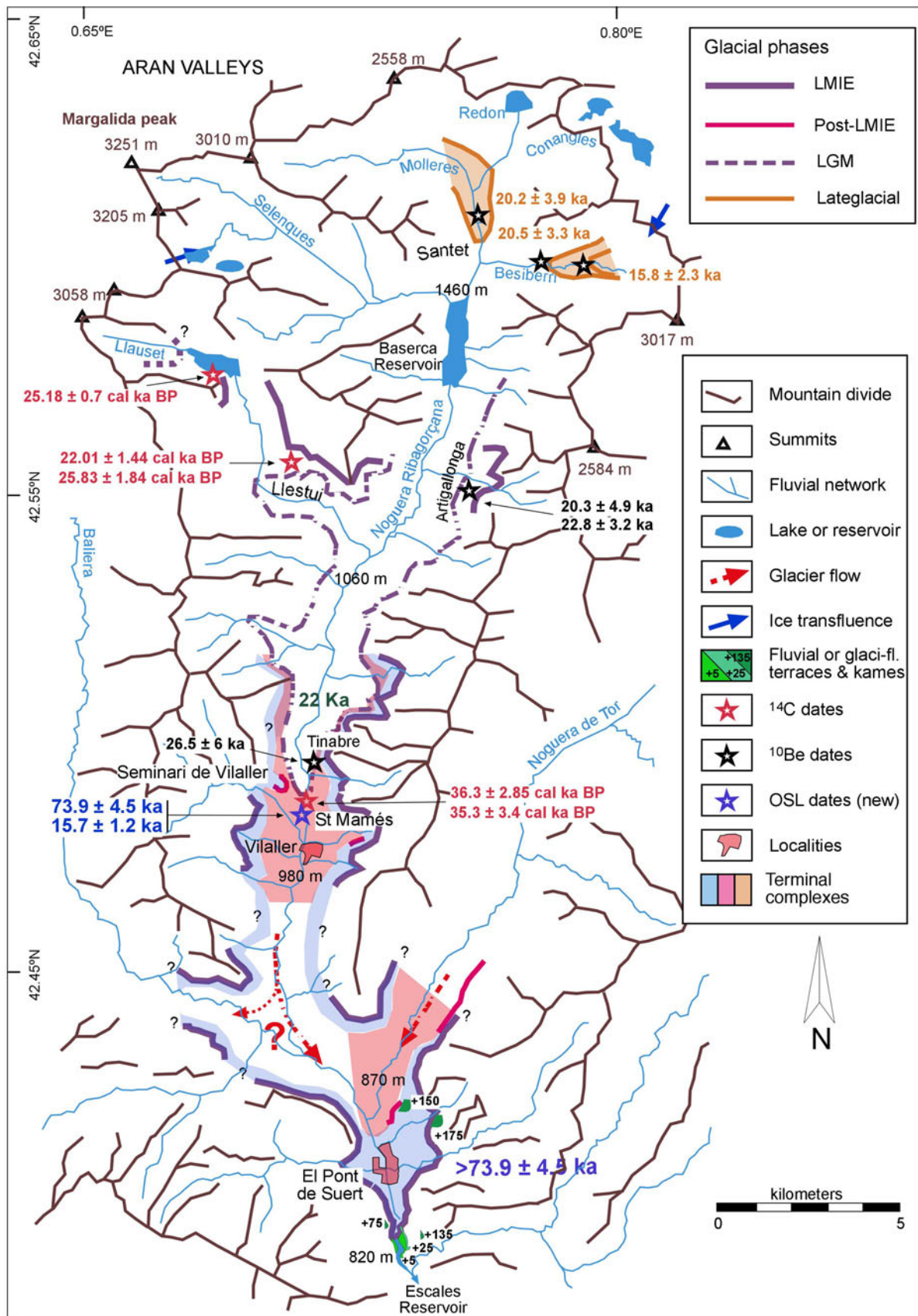
Figure 2. Geomorphological sketch of the upper Ribagorçana valley (reinterpreted from Mey, 1965; Vilaplana, 1983a). Relevant [10]Be samples from Pallàs et al. (2006) were recalculated. Bulk carbon samples from Vilaplana (1983a) at Llauset, Vilaplana and Bordonau (1989) at Llestui, and Bordonau (1992) at the Seminari de Vilaller. LMIE, last maximum ice extent; LGM, last glacial maximum; OSL, optically stimulated luminescence.
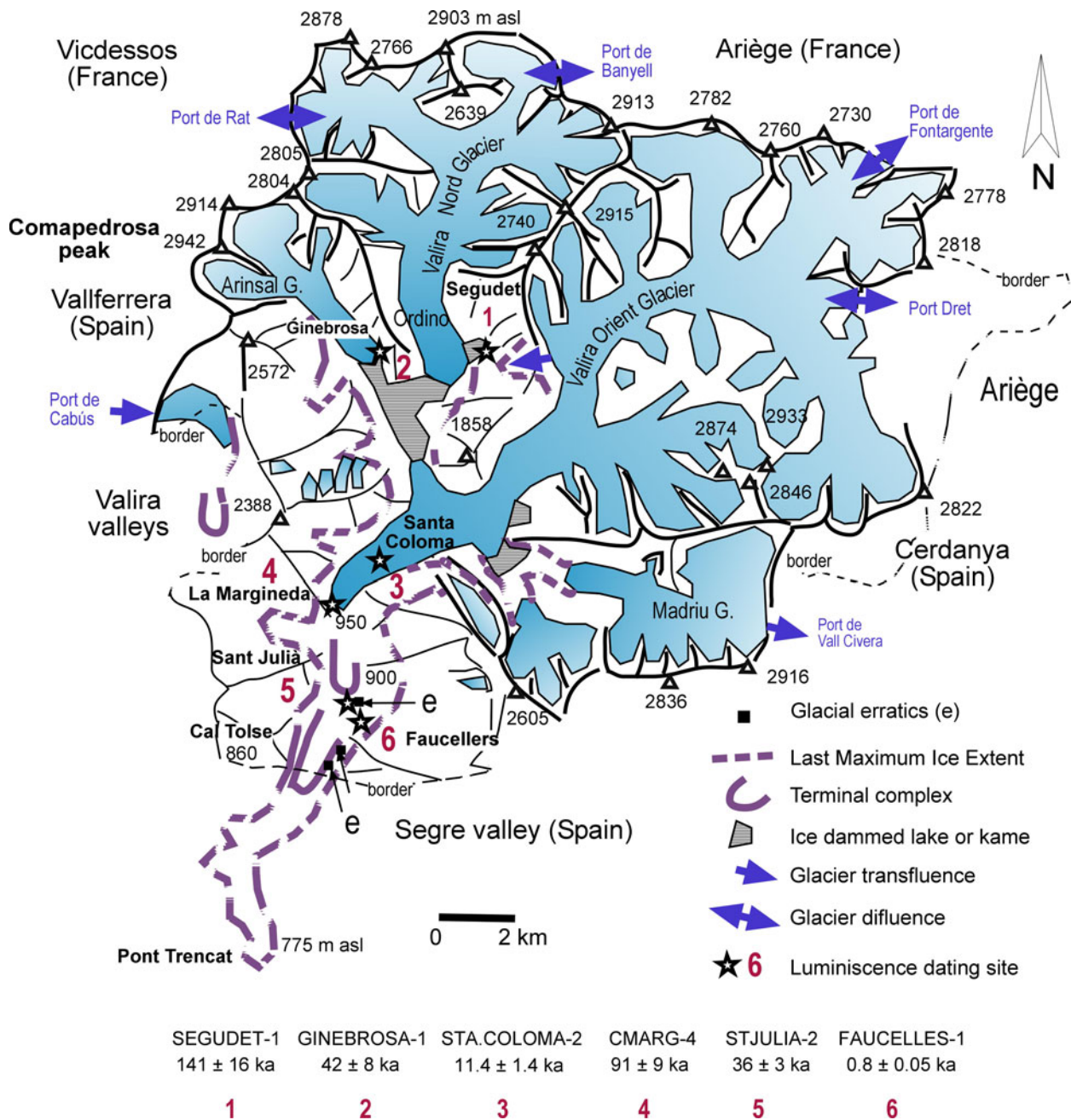
Figure 3. Andorra glacier extension (adapted from Turu et al., 2017) and sampled site position (Fig. 1, sector 3). The blue colour represents the ice extension. (1) SEGUDET-1; (2) GINEBROSA-1; (3) STA.COLOMA-2; (4) CMARG-4; (5) STJULIA-2; and (6) FAUCELLES-1.

kames, to obtain dates. According to Turu and Bordonau (1997), the Segudet and Ginebrosa kames were formed when the Arinsal and Ordino glaciers converged to form a single ice tongue on palaeo-Lake La Massana (1250 m asl) (Turu et al., 2017).

The upper Segre and Cerdagne

In the upper Segre and Cerdagne basin (Fig. 1, sectors 3 and 4), exposures are found at the confluence of the Segre River with its tributaries (Adrall and Ur sites) or within the Segre River terrace system (Sanavastre).

At Adrall, a fluvial terrace is located near the confluence between the Segre and its tributary, Castellbó, which exclusively

drains low-grade metamorphic rocks (Hartevelt, 1970). The Adrall terrace is far from any glacial front; however, it belongs to the glaciofluvial Segre–Valira terrace system (+38 m arb) and has been correlated with the Cal Tolse terminal complex (Turu and Peña-Monné, 2006; Turu et al., 2007; Peña-Monné et al., 2011).

The Cerdanya is located in the uppermost part of the Segre basin and drains low-grade metamorphic rocks and granites on its northern border (ICGC, 2006). This area was divided by the treaty of the Pyrenees in 1659, so we use "Cerdagne" for the French part (in the north) and "Cerdanya" for the Spanish zone. Within the latter area, we found the abandoned quarry of Albellorols (1060 m) close to the village of Sanavastre, in which a weathered coarse deposit, some 7-8 m thick, is located
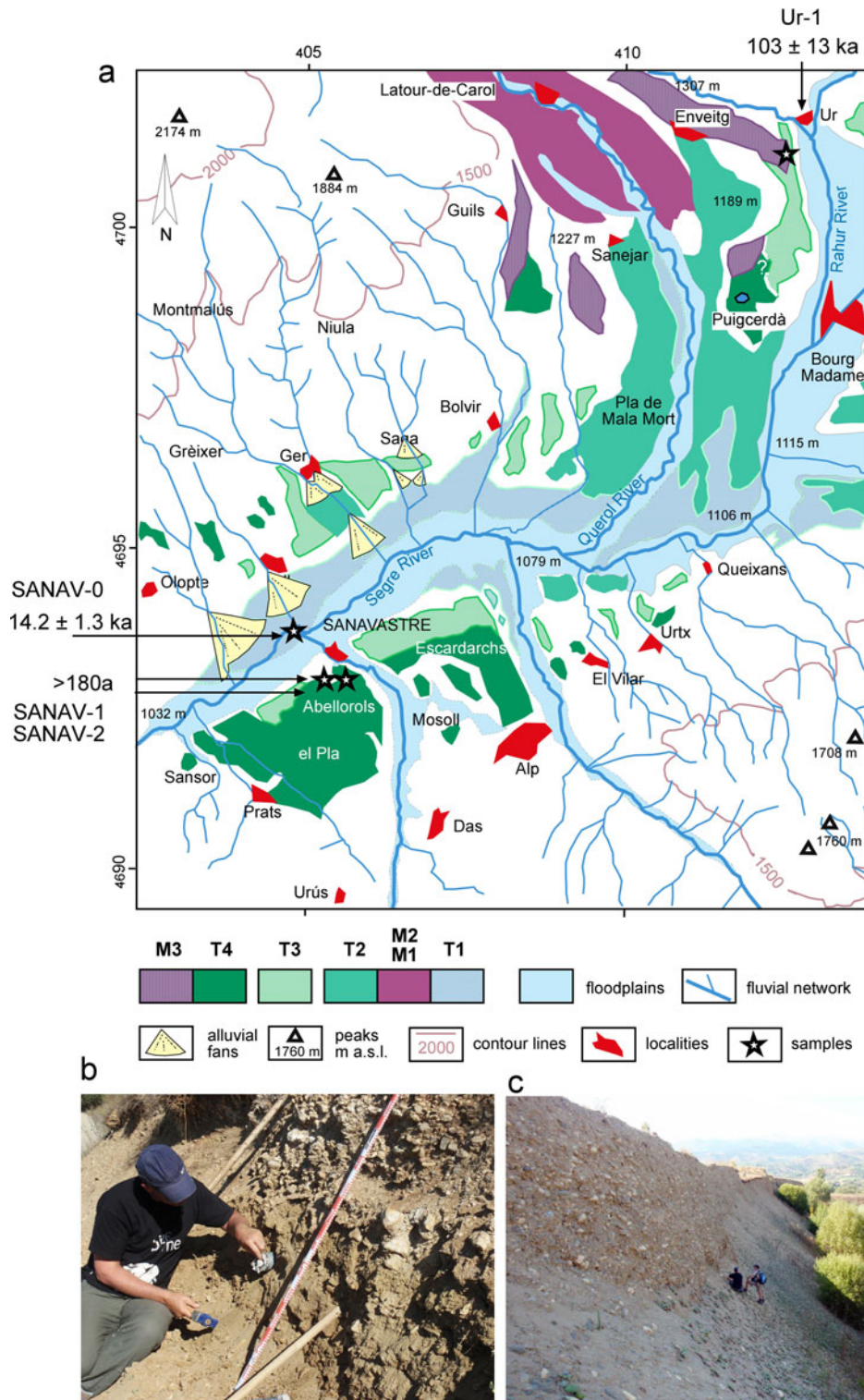
Figure 4. (a) Quaternary facies from the Cerdanya basin after ICGC (2006) geological map, modified for this work. Moraines (M) and associated terraces (T). Location of the samples for optically stimulated luminescence (OSL) dating: (b) sampling for OSL dating at the Abellorols lignite quarry (near Sanavastre) from deposits of a Segre fluvial terrace, sample SANAV-1 from the upper division; (c) sample SANAV-2 from the lower division.

at ∼20–35 m arb and belongs to the Segre T4 (the Mala Mort level; Calvet, 1998). Terrace T4 overlapped by the Escadarchs fan (Fig. 4) and was fed by limestone-sourced sediments. In Cerdagne, T4 is decalcified by intense weathering (Calvet, 1998), but this is not the case for the same terrace on the southern flank of the Segre River (Poch et al., 2013). The fluvial

terrace system continues downstream in the form of two weathered outliers (terrace T3; Fig. 4). Pedogenic geopetal structures, including carbonate nodules and minor clay accumulation, are common in terrace T3 (Poch et al., 2013), with gruss from weathered cobbles of granite; however, rich-iron minerals remain unweathered.

The well-known nested end-moraine complex of the Carol glacier surrounding Puigcerda is found in Cerdagne (Calvet, 1994, 1998; Calvet et al., 2011b; Pallàs et al., 2010 and references therein; Fig. 4). Upstream of the Carol–Segre confluence is the Ur-Llaurar rest area (Fig. 4) close to the N20 highway, in which we sampled a sandy layer from a thick deposit of glaciofluvial gravels.

MATERIALS AND METHODS

Fieldwork

Fieldwork included detailed geological characterisation of each exposure, consisting of stratigraphic logging and interpretation of sedimentological features. Sample collection (Table 1) from previously cleaned profiles was undertaken at the sites mentioned above (Fig. 1) from coarse glaciofluvial, colluvial, or fine-grained glaciolacustrine sediments. For luminescence dating, we hammered steel tubes into the sections and then extracted them, avoiding any exposure of the contents to daylight. Adjacent to each tube, a subsample of sediment was collected to determine the dose rate at the laboratory.

Grain-size analysis

The texture of the sediment samples was determined at the Sedimentology Laboratory of the Department of Earth Sciences, University of Coimbra, Portugal (Supplementary Material 1). The grain-size distribution and statistical parameters of each sample were obtained through the integration of two methods: by sieving the >63 μm fraction and by laser diffraction analysis of the <63 μm fraction with a Coulter laser granulometer (2 mm–0.04 μm). The grain-size distribution provides information about the sediments' maturity, transportation history, and deposition. Because particles transported under subaerial conditions are exposed to daylight, near-complete bleaching (zeroing of the optically stimulated luminescence [OSL] signal during transport) is expected, avoiding luminescence-dose inheritance (see Hoey, 2004). Sediments suitable for OSL are those of fluvial or aeolian origin, showing skewed, unimodal, well-sorted grain-size distributions and associated with transport histories in which subaerial conditions are met. Because such ideal conditions would not always be represented in a glacial-type or related deposit (Walker, 2005), two modern samples from the Segre riverbed were measured to estimate the offset of possible inheritances (Table 1, SANAV-0 and STPCodinet-1).

Water-content estimations

For each sample, we calculated the field water content (w). First, we estimated the void ratio (e), a parameter related to packing the particles within the sediment. This parameter is readily estimated concerning published tables (Jiménez-Salas and de Justo-Alpañes, 1975). For example, $e = 0.35$ equates with the densest packing of spherical particles of equal size bearing on top of each other, whereas $e = 0.91$ corresponds to the weakest packing of spheres. The void ratio and the porosity (n) are related by $n = e \ (1 + e)^{-1}$. Because the density of igneous and metamorphic particles forming the framework of unconsolidated sands are known ($\rho \approx 26.5$ kN/m^3), the dry density (δ_d) is associated to the porosity (n) related by $\delta_d = \rho \cdot (1 - n)$, while the density of a fully saturated soil (δ_s) is: $\delta_s = \delta_d + n \cdot \delta_w$, where δ_w is the density of liquid water. Estimating the water content (w%) at full saturation may also be

an estimate of the maximum water content during the burial period, probably below the water table; thus $w\% = 100 \cdot (\delta_s - \delta_d) \cdot \delta_d^{-1}$. However, once the deposits have been uplifted or exposed by erosion, the water content will be lower than in fully saturated conditions. The minimum water content corresponds with the highest void ratio because these are inversely related. When the deposits are unsaturated, capillarity action retains moisture at a rate inversely proportional to their void ratio. Void ratio values for the most common deposits are shown in Supplementary Material 2. Knowledge of water content is important, as water absorbs radiation differently from mineral sediment and thus must be accounted for in dose-rate calculations (Walker, 2005).

Luminescence dating

In this section, we include both OSL and thermally stimulated luminescence methods. We dated several deposits twice to identify any biases between these methods. Luminescence dating covers those analytical methods that measure the time elapsed since grains of particular minerals (e.g., quartz or feldspars) were last exposed to significant heating or daylight (Duller, 2004). The method was developed mainly by using quartz as the dose meter (Qtz-OSL), but K-feldspar can be used when the Qtz-OSL signal is saturated.

OSL dating

Exposure to daylight during sediment transport removes the latent luminescence signal from the quartz or feldspar crystals. After the burial, the luminescence signal (trapped charge) starts to accumulate in the mineral grains due to ionising radiation arising from the decay of ^{238}U, ^{232}Th, and ^{40}K present in the sediment and from cosmic-ray bombardment (Murray et al., 1987). In the laboratory, the equivalent dose (D_e, assumed to be the dose absorbed since the last light exposure; i.e., the burial dose, expressed in Gy) is determined by comparing the natural luminescence signal resulting from the charge trapped during a burial with that trapped following laboratory irradiation (Olley et al., 1996). For the calculation of the dose rate of sand-sized K-feldspar grains, an internal K content of $12.5 \pm 0.5\%$ was assumed (Huntley and Baril, 1997).

Sample preparation for luminescence analyses was undertaken in darkroom conditions. Samples were wet-sieved to separate the 180–250 μm grain-size fraction, followed by HCl (10%) and H$_2$O$_2$ (10%) treatments to remove carbonates and organic matter, respectively. The K-feldspar–rich fraction was floated off using a heavy-liquid solution of sodium polytungstate (density = 2.58 g/cm^3). The quartz fraction was obtained by etching another portion with concentrated hydrofluoric acid (HF) (40%). The K-feldspar fraction was treated with 10% HF for 40 minutes to remove the outer alpha-irradiated layer and clean the grains. After etching, the quartz and K-feldspar fractions were treated with hydrochloric acid (HCl) (10%) to dissolve any remaining fluorides. Quartz purity was confirmed by the absence of a significant infrared-stimulated luminescence (IRSL) signal.

Equivalent doses were measured on automated Risø TL/OSL DA-20 readers, each containing a beta source calibrated for irradiation on stainless steel discs and cups. Quartz measurements were made on large (8 mm) aliquots containing several thousands of grains mounted on stainless steel discs. Small (2 mm) aliquots of K-feldspar were mounted on stainless steel cups. Quartz dose estimates were made using a standard single-aliquot regenerative-

Table 1. Optically stimulated luminescence (OSL) dating results obtained by the Nordic Laboratory for Luminescence Dating (NLL).[a]

NLL code	Field code	m arb	m asl	Depth (m)	Grain size	Age (ka)	Protocol	Dose (Gy)	n	Dose rate (Gy/ka)
122235	SANAV-0	+0	1045	0.05	VCS	0.45 ± 0.05	Quartz-OSL	1.34 ± 0.14	21	3.00 ± 0.11
122235	SANAV-0	+0	1045	0.05	VCS	14.2 ± 1.3	pIRIR290	56 ± 5	12	3.91 ± 0.12
122236	SANAV-1	+38	1080	1.25	FS	>69 ± n/a	Quartz-OSL	>250	1	3.63 ± 0.13
122236	SANAV-1	+38	1080	1.25	FS	>180	pIRIR290	>800	6	4.52 ± 0.14
122237	SANAV-2	+29	1075	10	MLS	>77	Quartz-OSL	>250	1	3.25 ± 0.12
122237	SANAV-2	+29	1075	10	MLS	>200	pIRIR290	>800	11	4.11 ± 0.13
122238	VILALLER-1	+10	972	2.5	CS	15.7 ± 1.2	Quartz-OSL	40 ± 2	27	2.53 ± 0,12
122239	VILALLER-2	+12	974	0.5	CS	73.9 ± 4.5	Quartz-OSL	83 ± 3	37	1.13 ± 0.05
122240	UR-1	+40	1226	20	CS	103 ± 13	pIRIR290	543 ± 62	10	5.30 ± 0.21
122241	SORT-1	+35	700	17	MS	>49 ± n/a	Quartz-OSL	>200	3	4.08 ± 0.19
122241	SORT-1	+35	700	17	MS	>162	pIRIR290	>800	3	4.94 ± 20
122242	STA.COLOMA-2	+15	975	2	CMS	11.4 ± 1.4	Quartz	44 ± 5	16	3.86 ± 0.17
122243	CMARG-4	+65	990	10	MLS	91 ± 9	pIRIR290	519 ± 48	10	5.72 ± 0.22
122244	STJULIA-2	+20	890	1.5	FS	36 ± 3	pIRIR290	205 ± 16	9	5.67 ± 0.22
122245	SEGUDET-1	+200	1500	6	LFS	141 ± 16	pIRIR290	592 ± 62	17	4.20 ± 0.16
122246	FAUCELLES-1	+10	1131	28	BS	0.81 ± 0.05	Quartz	4.32 ± 0.12	33	5.34 ± 0.25
122247	ADRALL-4	+35	625	2.8	MLS	179 ± 15	pIRIR290	843 ± 62	22	4.70 ± 0.15
122248	STPCodinet-1	+0	593	0.05	MS	0.19 ± 0.03	Quartz	0.59 ± 0.09	27	3.08 ± 0.11
122256	GINEBROSA-1	+200	1449	6	LS	42 ± 8	pIRIR290	151 ± 30	18	3.63 ± 0.13

[a]Abbreviations: arb, above riverbed; asl, above sea level; BS, bioturbate silts; CMS, coarse-medium sand; CS, coarse sand; FS, fine sand; LFS, laminated fine sand; LS, laminated silts MLS, medium laminated sand; MS, medium sand; VCS, very coarse sand.

dose (SAR) protocol using blue-light stimulation at 125°C for 40 s with a 240°C preheat for 10 s, a 200°C cut the heat, and an elevated temperature (280°C) blue light–stimulated clean-out step (Murray and Wintle, 2000, 2003). The OSL signal was detected through a U-340 filter. All samples had a strong, fast component. The net OSL signal was calculated from the stimulation's initial 0.0–0.8 s and an early background between 0.8 and 1.6 s.

The K-feldspar D_e estimates were measured with a post-IR IRSL SAR protocol using a blue-filter combination (Thomsen et al., 2008; Buylaert et al., 2012). The preheat was 320°C for 60 s, and the cut heat was 310°C for 60 s. After preheating, the aliquots were IR bleached at 50°C for 200 s (IR50 signal) and subsequently stimulated with IR at 290°C for 200 s (pIRIR290 signal). It has been shown by Buylaert et al. (2012) that the post-IR IRSL signal measured at 290°C can give accurate results without the need for correction for signal instability. For all IR50 and pIRIR290 calculations, the initial 2σ of the luminescence decay curve, less a background derived from the last 50 s, was used. Dividing the D_e by the environmental dose rate (in Gy/ka) gives the luminescence age of the sediment.

Thermoluminescence dating
Samples were treated in the laboratory following conventional procedures for fine-silt (4–20 μm) sample preparation (Mauz et al., 2002) and etched using 20% and 10% HF for various rounds to remove the feldspar-derived luminescence component (Mauz and Lang, 2004a). After the grains were etched, the silt of 4–15 μm grain size was separated by settling in acetone. The aliquots of each sample consisted of 2 mg of material pipetted onto 1 cm aluminium discs. All samples were tested using infrared stimulation (Duller, 2003), which examines the effect of the feldspar on normalised thermoluminescence (TL) measurements and gives an estimate of the amount of feldspar remaining in the sample after chemical treatment (Mauz and Lang, 2004a). According to these tests, all samples used for further experiments were pure quartz. The self-attenuation of the samples was calculated in a simplified approach using the following equation:

$$D = DO \cdot (1 - \mu \cdot r/3)$$

Where D is the attenuated dose of gamma radiation, DO is the dose delivered by the source, μ is the linear attenuation coefficient of the sample, and r is the inner radius of the container. Equation 1 was derived for homogenous and isotropic radiation around a small container, compared with the mean free path of gamma photons ($\mu \cdot r \ll 1$). Any attenuation due to the thickness of the "sample" is assumed to result from a homogenous and isotropic radiation field. The 90–160 μm fraction was obtained by dry-sieving, and the 4–11 μm fraction was extracted by settling in acetone. TL measurements were performed using a blue detection window. Some measures were made with and without silicon oil as a fixing agent. An insignificant tendency toward slightly lower results with silicon was observed. All analyses were performed at the ITN (Instituto Tecnologico Nuclear, C2TN, Campus Tecnológico Nuclear, in Portugal, following laboratory procedures from Mauz and Lang (2004b) and Richter et al. (2003).

Radiocarbon accelerator mass spectrometry (AMS) dating
Radiocarbon AMS dating was restricted to bulk sediment samples from the Valira valleys. Measurement of ^{14}C activity and the isotope ratio ^{13}C/^{12}C was carried out at the Beta Analytic Inc.

(Florida, USA) mass spectrometer facility and used the bulk organic fraction from sedimentary samples. Calib software based on IntCal20 curves was used for calibration (Reimer et al., 2020). Because radiocarbon dating is routinely applied to the final part of the LGC and the Holocene (Walker, 2005), the method is explained in Supplementary Material 3.

RESULTS

Luminescence results are presented from west to east across the study area (Fig. 1), including the sedimentary records and their ages (Tables 1 and 2), while the radiocarbon (^{14}C) ages are exclusively from the Valira valleys (Table 3). Some deposits were sampled twice to assess the coherence between dating methods. These TL samples are LUM-26, LUM-273, and LUM-274 (Table 2); compared with OSL results of samples 122242, 122244, and 122247 (Table 1), respectively, which show good agreement.

Qtz-OSL dating provided finite ages only in a few ancient samples (122238, 122239, 122242, and 122246; Table 1) and two modern samples (122235 and 122248; Table 1) from the Segre River. In all the other samples, the Qtz-OSL signal was saturated or nearly saturated and only provided minimum ages (122236, 122237, 122240, 122241, 122243, 122244, 122245, 122247, 122256; Table 1). Therefore, signals from K-rich feldspars were used instead because of the higher saturation dose of the dose-response curve for feldspar (Wintle and Murray, 2006). The pIRIR290 signal was chosen because of its stability (Buylaert et al., 2012). We also made several direct tests of the stability of the pIRIR290 signal and checked the suitability of the applied measurement protocol and the completeness of signal bleaching at deposition by using modern samples (122235 and 122248; Table 1). The pIRIR290 signal of several samples is saturated or nearly so; only minimum ages were obtained (122236, 122237, and 122241; Table 1). More complete information about the laboratory measurements of the OSL samples is available in Supplementary Material 4.

Qtz-OSL dating provided finite ages in samples VILALLER-1, STA.COLOMA-2 and FAUCELLES-1 (Table 1), and the two current Segre River bed-load samples, SANAV-0 and STPCodinet-1. The Qtz-OSL signals were too close to saturation for suitable dating for all other samples. For older samples, signals from K-rich feldspars were used instead because of the higher saturation dose of the feldspar dose–response curve (Wintle and Murray, 2006). These samples are UR-1, CMARG-4, STJULIA-2, SEGUDET-1, ADRALL-4, and GINEBROSA-1 (Table 1). However, several samples were too close to saturation, and only minimum ages were obtained (SANAV-1, SANAV-2, and SORT-1; Table 1). Further empirical information about the offset and saturation of the luminescence signal is provided in Supplementary Material 5.

Results from the upper Noguera Ribagorçana valley

The results from the westernmost side of the studied area (Fig. 1, sector 1) are presented in this section. We briefly summarize the existing knowledge of the area and set our results in context. Radiocarbon dates performed on bulk sediment samples retrieved from glaciolacustrine sediments recovered by coring at a site 500 m north of Sant Mamés (Fig. 2) returned inverted ages (Bordonau, 1992). Contamination probably affected one or all of these samples, as was presumed to be the case with glaciolacustrine deposits from the Llestui lateral ice-dammed lacustrine

Table 2. Thermoluminescence (TL) finite ages from the studied deposits: Lum-24 to Lum-27 (from Turu and Peña-Monné, 2006), Lum-272 (from Gascón and Turu, 2011), Lum-273 (from Jalut and Turu, 2008), and Lum-274 (not published).[a]

ITN code	Field code	m arb	m asl	Depth (m)	Grain size	Age (ka)	Dose (Gy)	Dose rate (Gy/ka)
LUM-24	ADRALL-1	+145	735	4.0	Coarse sand	> 350	n.a.	~8.08
LUM-25	ADRALL-2	+124	714	2.0	Coarse sand	> 350	n.a.	~8.08
LUM-26	ADRALL-3	+35	625	2.8	Medium laminated sand	120 ± 6	1490 ± 39	7.73 ± 0.33
LUM-27	Cal Tolse	+85	964	3.0	Coarse sand	125 ± 14	1552 ± 144	8.43 ± 0.36
LUM-272	Pont Trencat	+15	800	3.0	Laminated silt	0.55 ± 0.03	6.5 ± 0.2	8.08 ± 0.34
LUM-273	STJULIA-1	+20	890	1.5	Fine sand	32.8 ± 1.2	384.7 ± 6.2	8.08 ± 0.34
LUM-274	STA.COLOMA-1	+15	975	2.0	Coarse sand	9.5 ± 0.3	116.8 ± 1.5	8.08 ± 0.34

[a]Abbreviations: arb, above riverbed; asl, above sea level.

complex (Bordonau et al., 1993), located upstream in the same valley (Fig. 2). The problem was apparently solved at Llestui, where Bordonau et al. (1993) reported two new ages (23,497–20,612 b2k and 27,671–23,993 b2k) from the LGM glaciolacustrine deposits (Pallàs et al., 2006).

The exposure of the abandoned Sant Mamés de Vilaller quarry has two divisions: a non-deformed glaciofluvial unit and a syn-sedimentary deformed unit. Within the deformed unit, lenses of laminated sand are embedded in a matrix-supported diamicton, which is interpreted as a melt-out till. An overlapping contact divides the Sant Mamés deposit into two units between glaciofluvial sediments that overlap a diamicton (Fig. 5a). The glaciofluvial unit is predominantly sandy but also includes layers of imbricated gravels, indicating that the sedimentation was influenced by episodes of high meltwater discharge (Fig. 5b). Within the diamicton, we identified a massive lodgement till at the base of the outcrop that grades to crudely bedded sands and gravels including boulders (Fig. 5c) (type C1b facies based on Krzyszkowski and Zieliński [2002]), whereas deformed sandy layers are interbedded at the top of the outcrop (Fig. 5d) (melt-out till facies; Bordonau, 1992).

A sample from the glaciofluvial unit provided an age of 15.7 ± 1.2 ka (VILALLER-1; Table 1), whereas the melt-out till gave an age of 73.9 ± 4.5 ka (VILALLER-2; Table 1). The time interval between these ages sheds light on an unconformity between the melt-out till and the later glaciofluvial unit. Further field descriptions are available in Supplementary Material 6.

Results from the upper Noguera Pallaresa Valley

The neighboring glaciated valley eastward from the upper Noguera Ribagorçana is the upper Noguera Pallaresa valley (Fig. 1, sector 2). In this valley, we analysed a glaciofluvial terrace exposure in Sort. Southward from the village of Sort (692 m), a 120-m-long outcrop was visible in 1992, on the right side of the widened N260 highway, revealing a glaciofluvial terrace (Peña-Monné et al., 2011; Ventura and Turu, 2022) at the toe of a large and currently inactive landslide (Turu et al., 2011). A sandy layer from this terrace was sampled for OSL dating (SORT-1; Fig. 6, Table 1) and provided a minimum age >162 ka. The sampled layer overlies coarser deposits and is partly eroded in its upper part (Fig. 6). From bottom to top, we distinguished massive and crudely bedded gravels arranged in sets of low-angle sheets at the bottom of the exposed deposit (Fig. 6); these are partly cut by erosion with a broad channel bar sheet

formed by imbricate massive gravels overlying its erosive surface. Crudely bedded sands deposited in low-angle sheets sit concordantly above the coarse deposits. Unfortunately, an unexposed section between this sandy layer and the top of the sequence prevented a complete determination of the stratigraphic record (Fig. 6). However, no significant changes in the sedimentary environment are apparent, there being a profusion of existing imbricated gravels in all visible parts of the sequence. At the top, a poorly consolidated coarse-grained diamicton marks the end of the sedimentary sequence at Sort.

We attribute the Sort deposit to a type C end-moraine fan, as described by Krzyszkowski and Zieliński (2002). The crudely bedded gravels at the base of the deposit corresponding to facies C1a, the channel bars to C1b, and the low-angle sand sheet to C2a. The broad range of facies represents a proximal end-moraine fan (Krzyszkowski and Zieliński, 2002), above which are the remains of the frontal moraine (uppermost facies B1b; Fig. 6).

Results from the Valira valleys

The Valira River joins the Segre at La Seu d'Urgell (Fig. 1, sector 3). Its basin (592 km^2) covers most of the Principality of Andorra (Fig. 3).

The Segudet kame

The Segudet kame complex is located at the confluence of the Cassamanya and Les Aubes streams (Fig. 7a). A subglacial till deposited at Segudet (1350 m; Fig. 7a) may indicate the limits of the ice-dammed valley impounded by the Ordino glacier (Turu et al., 2017). A supraglacial till exists on the hillslope (1520 m; Fig. 7b), deposited by the 200-m-thick trunk glacier. The kame comprises thick glaciofluvial gravels, mainly located in its central part. It is possible to trace this gravely unit to the edge of the sedimentary complex, where it grades to sands and silts. The OSL sample was taken from a laminated fine sand layer (Fig. 7c and d) and provided an age of 141 ± 16 ka (SEGUDET-1; Table 1). Complementary field descriptions are provided in Supplementary Material 6.

The Ginebrosa kame

The Ginebrosa deposits are found 200 m above the Arinsal riverbed (1449 m; Fig. 3) and are related to a large kame terrace formed in a lee-side position between the Arinsal glacier (Fig. 3) and adjacent bedrock. Silts and sand lenses are located away from the former slope–glacier ice contact (Fig. 8a). These

Table 3. Radiocarbon dating results from Ginebrosa (β-133971, colluvium) and La Margineda sites (β-489299 organic fraction from colluvium; β-489301 organic fraction from carbonated silts).[a]

Lab. ref.	Name	Latitude	Longitude	asl	Depth	Sediment	Age yr BP	δ13C	Age yr cal BP
β-133971	Ginebrosa-2	N42°33′14.2″	E1°30′54.6″	1445 m	10.0 m	C	7360 ± 70	−26.8 ‰	8178 ± 155
β-489299	LM1 (Margineda)	N42°29′10.1″	E1°29′21.23″	1007 m	6.0 m	BK	22,290 ± 90	−26.6‰	26,645 ± 296
β-489301	LM2b (Margineda)	N42°29′06.37″	E1°29′20.42″	1007 m	3.0 m	Of	13,323 ± 40	−24.7‰	16,016 ± 171

[a]Calibration using IntCal20 (Reimer et al., 2020), δ13C carbon isotopic fractionation. asl, above sea level; BK, bulk organic matter; C, colluvium; Of, organic fraction.

lenses are interbedded with colluvium from nearby bedrock erosion. On the opposite side of the kame deposits, close to the former ice contact, deformed sediments include intrusions of cohesive clay lenses.

This small valley has been accessible since 1997, and several outcrops created by building work have been available for analysis. The sedimentary sequence was emplaced directly over polished bedrock from a previous MIE of unknown age (Fig. 8b, 1). Four sedimentary units were identified (Figure 8b, 2–5). Sandy lenses (Shr) and horizontally bedded imbricated gravels (Gt) form the lowermost unit (Fig. 8b, 2), draped over the bedrock and covered by massive gravels (Gm) beneath a diamicton layer (Dmm, Dcs) deposited by a glacial advance. A final sedimentary unit (Fig. 8b, 3), overlapped by sands and silts (Sh) grading to coarse gravels (Gp facies) (Fig. 8b) filled the irregular surface (Catuneanu, 2006; Fig. 8b, MRS). Instability caused by lateral glacial thrusting produced lenticular injections of cohesive clay. The age of the interbedded laminated sand lenses is 42 ± 8 ka (GINEBROSA-1; Table 1). A Holocene postglacial unit (Fig. 8b, 5) formed by fine-grained colluvium gave dates of 9.17 ± 0.15 ka cal BP using a 14C AMS determination on bulk organic matter (GINEBROSA-2; Table 3).

The Santa Coloma quarry
In the Santa Coloma terminal complex (Fig. 9a), several fining-upward fluvial sequences deposited from high-energy floods (Fig. 9b) were described by Turu and Peña-Monné (2006). Two field campaigns in December 2005 (Fig. 9a and c) and September 2011 (Fig. 9b) were conducted to collect luminescence dating samples. Respective results are quite similar: 9.5 ± 0.3 ka using TL (STA.COLOMA-1; Table 2) and 11.4 ± 1.4 ka using OSL (STA.COLOMA-2; Table 1). Further field descriptions are available in Supplementary Material 6.

La Margineda
The main Andorran valley becomes narrower southward of Santa Coloma (Fig. 10a), and an urbanized hill, known as La Margineda (990 m), stands on the valley's eastern side eastern. We examined an existing outcrop rich in sedimentary facies located at +65–75 m arb (1008 m asl) in a road cutting (Fig. 10b). Here, colluvial facies overlie a glaciofluvial deposit, both densely compacted (Fig. 10c), from which samples were collected (Fig. 10c) for AMS and luminescence determinations. Two sedimentary discontinuities are identified in the road cut (Fig. 10d), differentiating three units (Fig. 10e). The lowermost unit, sampled for OSL dating, comprises imbricated gravels with a significant presence of allochthonous lithologies (e.g., granites), probably transported as bedload by meltwater mixed with colluvium from a melting glacial front and the end-moraine (Llobet, 1947; Turu and Peña-Monné, 2006) reworking. This unit is from MIS 5c (91 ± 9 ka;

CMARG-4; Table 1); however, the mentioned end-moraine buildup occurred earlier, probably during MIS 5d. In the middle unit (Fig. 10e), clasts are arranged with their long axes parallel to the slope (colluvium). However, some clasts are imbricated, and others set as though belonging to palaeochannels (lower unit). The occasional presence of allochtonous lithologies (e.g., granites) may come from the erosion of the terminal-moraine complex. The age of the colluvium (Fig. 10e, LM-1) is 26.931–26.201 ka cal BP (22.290 ± 0.090 ka BP; ß-489299; Table 3). The upper unit (Fig. 10e) is formed mainly by angular locally sourced gravels supported by a sandy-silt matrix belonging to the slope's current scree. The general glacial recession from La Margineda predated the deposition of the upper unit (unit 3; Fig. 10e). We were able to date this last unit in an existing road cutting 100 m south of the one described above. Here, unit 3 is very coarse and may come from a rock avalanche. We could date the matrix of this rock avalanche deposit using 14C AMS. The age of unit 3 is 16.018 ± 0.183 ka cal BP (sample LM2b; Table 3). These stratigraphic units belonging to MIS 2 are also identified 650 m southward from La Margineda, in Aixovall (Fig. 3, sector 3) from an existing open pit excavation (Fig. 11). Complementary field descriptions are provided in Supplementary Material 6.

The Sant Julià de Lòria outcrop
The village of Sant Julià de Lòria (900 m) is located in a V-shaped valley (Fig. 12). Here, the narrow Valira valley is a fluvial gorge carved in calcshists running southward from La Margineda. Cross-stratified sands were dated using TL and OSL (Fig. 13a). When error bars are considered, the dates from different methods converge: the TL age is 32.8 ± 1.2 ka (STJULIA-1; Fig. 13b, Table 2), and the OSL age is 36 ± 3 ka (STJULIA-2; Fig. 13c, Table 1). Geotechnical boreholes for a new bridge connecting a local road to the highway (Fig. 13d, profile) allowed us to identify a glacial diamicton 6 m beneath the Valira riverbed and beneath the studied exposure. The dated melt-out till (Fig. 13d, Till 2) should be younger than the diamicton located beneath the riverbed (Fig. 13d, Till 1). A previous southward terminal glacial-front position is deduced by erratics accumulated on the eastern margin of the valley at Cal Tolse (Fig. 12) and farther down the valley (Fig. 3), close to the Spanish–Andorran border (Bastida de Ponts glacial front; Fig. 3), but in an inner position regarding the LMIE far-flung moraine (Barr and Lovell, 2014) at Pont Trencat (Turu et al., 2007, 2017; Fig. 3). Further field descriptions can be found in Supplementary Material 6.

Results from the upper Segre

This section refers to three exposures, one close to the River Segre and two in the Cerdanya depression.
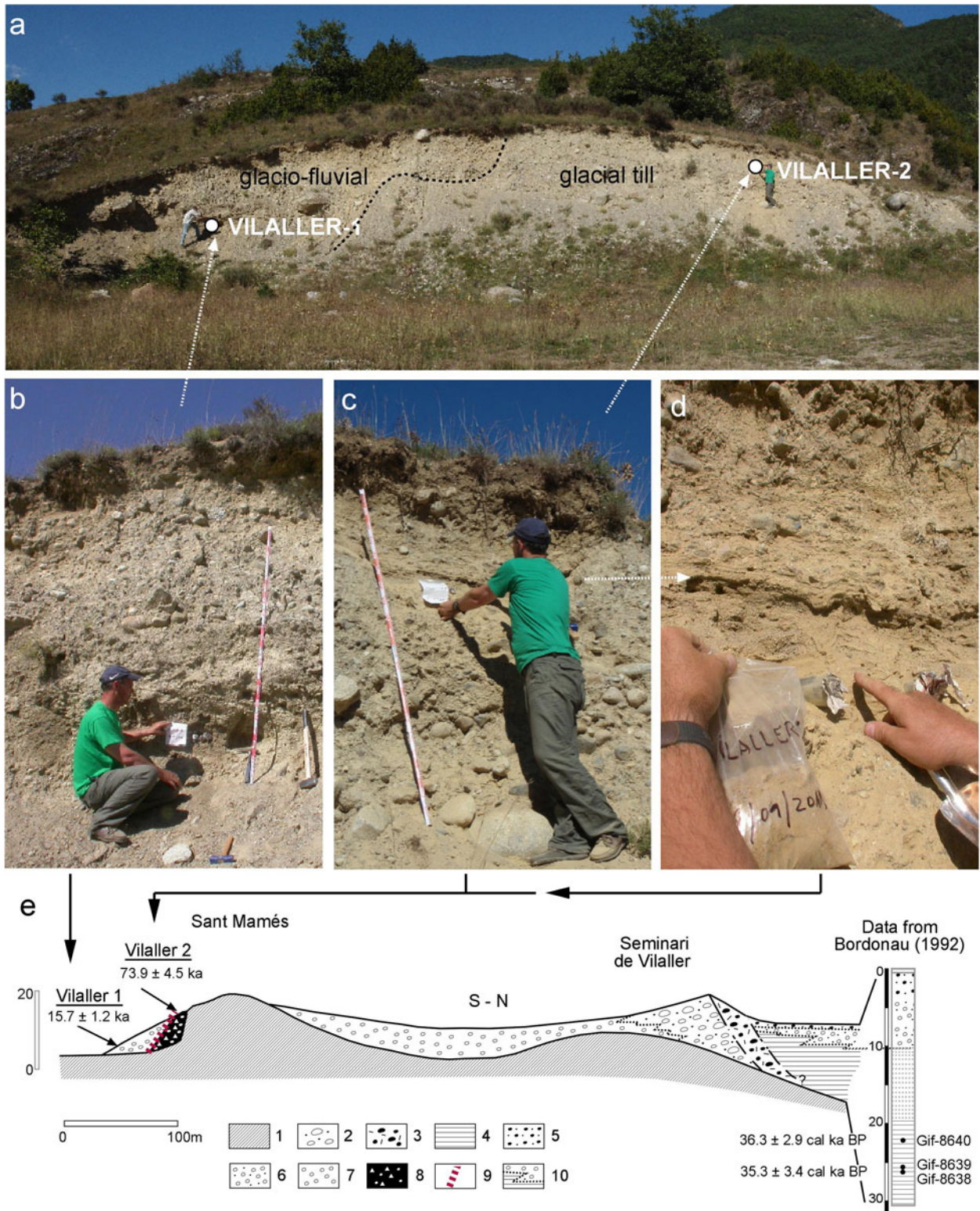
Figure 5. (a) Sketch of glaciofluvial deposits overlapping (dashed line) the glacial till (Fig. 1, sector 1). Collected samples are VILALLER-1 and VILALLER-2; (b) the western side of the Sant Mamés outcrop; (c) the eastern side of the Sant Mamés outcrop; (d) a closer look at the sampled layer embedded in the diamicton; (e) Sant Mamés outcrop. The interpretative section from Bordonau (1992) was modified and enlarged, with the location of the new optically stimulated luminescence (OSL) samples added. Accelerator mass spectrometry (AMS) ^{14}C ages are available from a borehole made in the early 1990s and plotted conformably at its vertical scale (Gif-8638: 30.8 ± 1.4 ka BP; Gif-8639: 20.18 ± 0.35 ka BP; and Gif-8640: 31.41 ± 1.2 ka BP; only valid calibrated ages are shown). 1, Rock basement; 2, supraglacial sediments; 3, lodgement; 4, bottom set (lacustrine facies); 5, fluvial; 6, topset (prograding fluvial facies); 7, outwash facies (glaciofluvial); 8, melt-out till; 9, unconformity; 10, facies changes. The black arrows indicate the location of the photographs in part e.
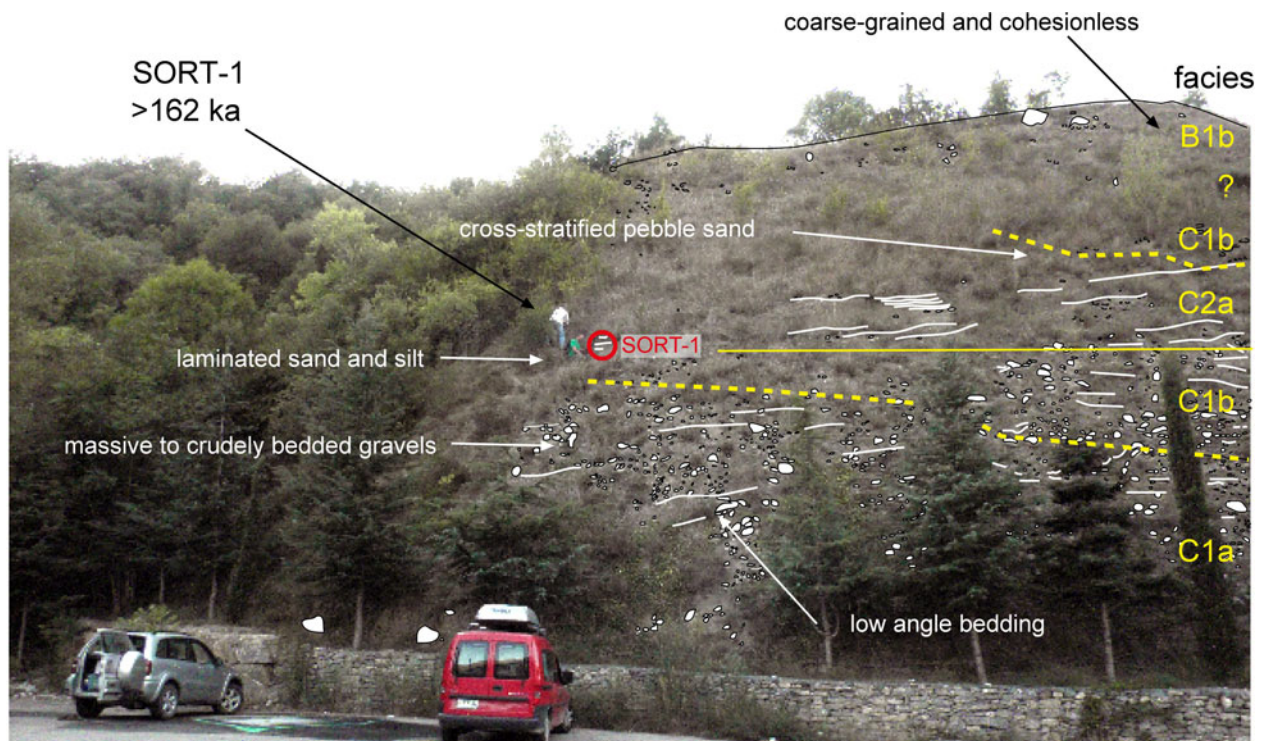
Figure 6. Sample site for optically stimulated luminescence (OSL) dating (SORT-1) at the Noguera Pallaresa glaciofluvial terrace +40 m at Sort (Fig 1, sector 2). Yellow lines = oriented layers; facies C1a = bedded gravels; C1b = channel bar, C2a = low-angle sands sheet; B1b = coarse-grained proximal end-moraine fan.

The upper Segre at Adrall

The exposure here is located 4.5 km below the Valira–Segre confluence (Fig. 1, sector 3). In Adrall (635 m asl), a 75-m-long outcrop was opened in 1986 during the widening of the N260 highway; however, it was not until 30 years later that the fluvial deposits were studied (Turu and Peña-Monné et al., 2006) and were shown to belong to the glaciofluvial Segre–Valira terrace system (Turu et al., 2007; Peña-Monné et al., 2011). The lowermost terrace level at Adrall (+38 m arb) incorporates three fining-upward sequences, each starting above an erosive surface (Fig. 14). These sequences grade upward from granite-rich gravels of Segre origin to schist-rich deposits of local derivation (Fig. 14). The whole terrace has been reddened by advanced weathering of iron minerals (oxidation), coatings, and meniscuses. TL ages (ADRALL-3; Table 2) are 120 ± 5.5 ka, but older ages were obtained using the OSL pIRIR290 procedure (179 ± 15 ka; ADRALL-4; Fig. 14, Table 1).

The upper Segre at Sanavastre

In the southern part of the Cerdagne basin (Fig. 1, sector 4), the Abellorols quarry in Sanavastre provided appropriate outcrops for OSL sampling in cross-stratified sandy layers surrounded by lenses of large cobbles. Samples from two levels (SANAV-1 and SANAV-2; Fig. 4b and c, Table 1) proved to be older than 200 ka. Available field descriptions are provided in Supplementary Material 6.

The Ur-Llaurar rest area

The Ur exposure is located 3 km above the Rahur–Segre confluence, on the eastern side of the N20 highway at the French village of Ur (Fig. 1, sector 4). An ancient quarry from the French N20 highway widening work in the mid-1980s was restored in a rest area. Exposures reveal several units (Fig. 15) of glaciofluvial channel deposits (units 1, 2, 4, and 5) and diamictons (units 3 and 6) belonging to an old glaciofluvial terrace from the Segre–Rahur river system (Fig. 4). The lowermost layer, unit 1, is a gravelly layer with trough cross-bedding. In contrast, unit 2 is a pebbly sand body with some imbricated rolled cobbles in an ochrous sandy matrix and with a ribbon geometry. It was partly eroded before or during the emplacement of the overlying units 3 and 4. An intercalated sand layer was dated to 103 ± 13 ka (UR-1; Table 1). Unit 3 is a massive diamicton with angular boulders, and unit 4 is composed of cross-stratified gravels with intercalated sheet sands. Unit 5 is mainly formed by gravels following a trough cross-bedding pattern, with a maximum thickness of several tens of meters. Unit 6 corresponds to a diamicton that includes striated clasts (Calvet et al., 2013).

Correlation between valleys

Based on AMS ^{14}C dates from kame deposits and in situ [10]Be CRE ages from both erratic boulders and moraines, the LGM phase is now well-defined in the eastern Pyrenees (Delmas, 2005; Delmas et al., 2008; Pallàs et al., 2010; Palacios et al., 2015; Turu et al., 2017). However, the number and the magnitude of glacial recession events during the LGC, their chronology, and those of the PGC still remain obscure.

In the studied area, the new OSL ages confirm glacial sedimentary records from MIS 6 to late MIS 2; nonetheless, glaciations older than MIS 6 are also indicated in the region. In the upper Noguera Pallaresa basin, the glaciofluvial terrace (+30–40 m arb) at Sort (Fig. 6) is older than 162 ka (Table 1). At Sanavastre (Fig. 4), +35–40 m and +25–30 m terrace levels are
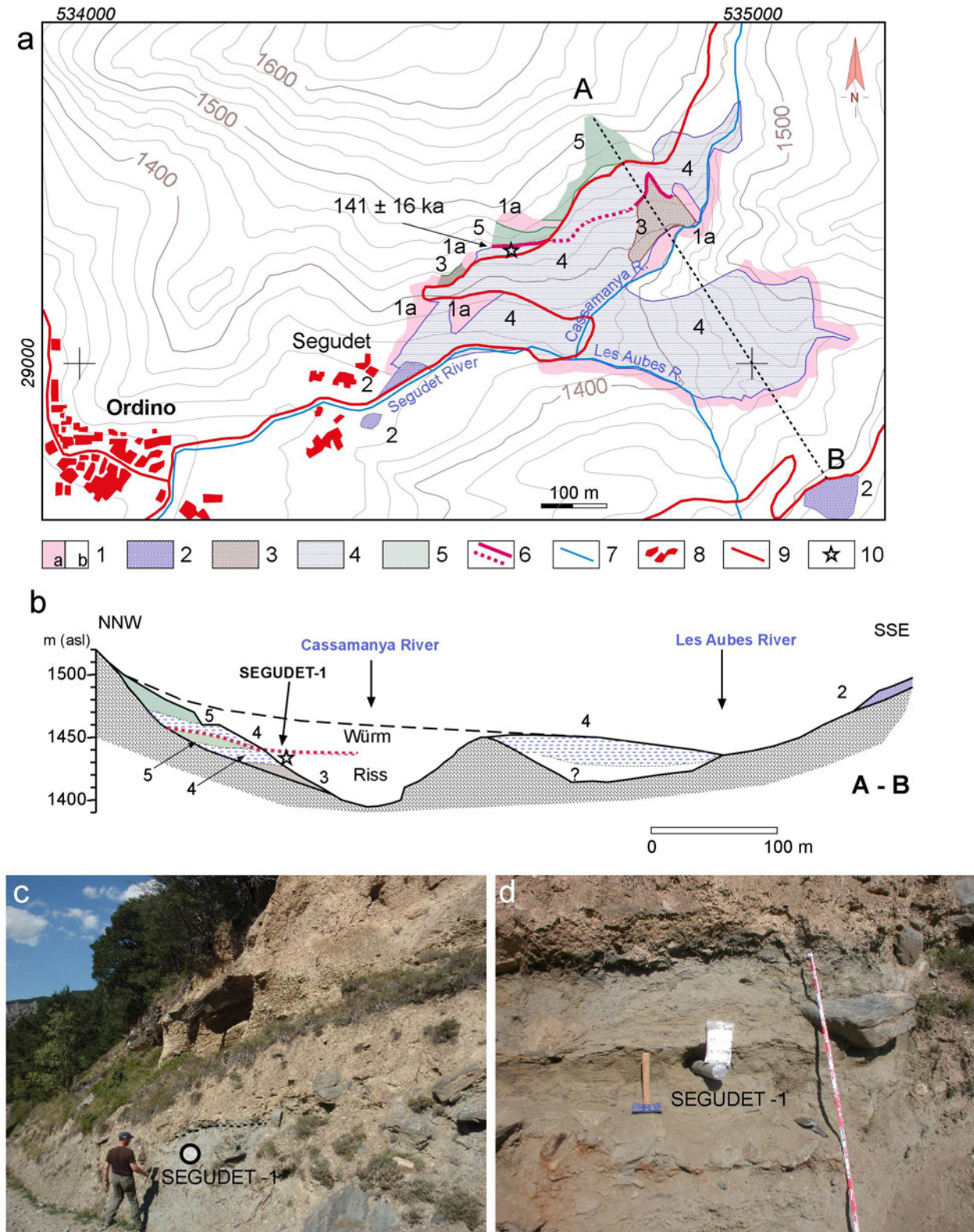
Figure 7. (a) Facies from the Segudet sedimentary sequence (Fig. 1, section 3). 1a, undifferentiated bedrock; 1b, not exposed; 2, diamicton; 3, glaciofluvial kame terrace laying over a polished surface; 4, glaciolacustrine deposits; 5, stratified colluvium; 6, identified unconformity (erosive surface) or supposed; 7, streams; 8, buildings; 9, road; 10, OSL sampling site. (b) Cross section (A-B) and location of sample SEGUDET-1 collected from rhythmites of the kame terrace complex. (c and d) Pictures of the stratigraphic position of sample SEGUDET-1.
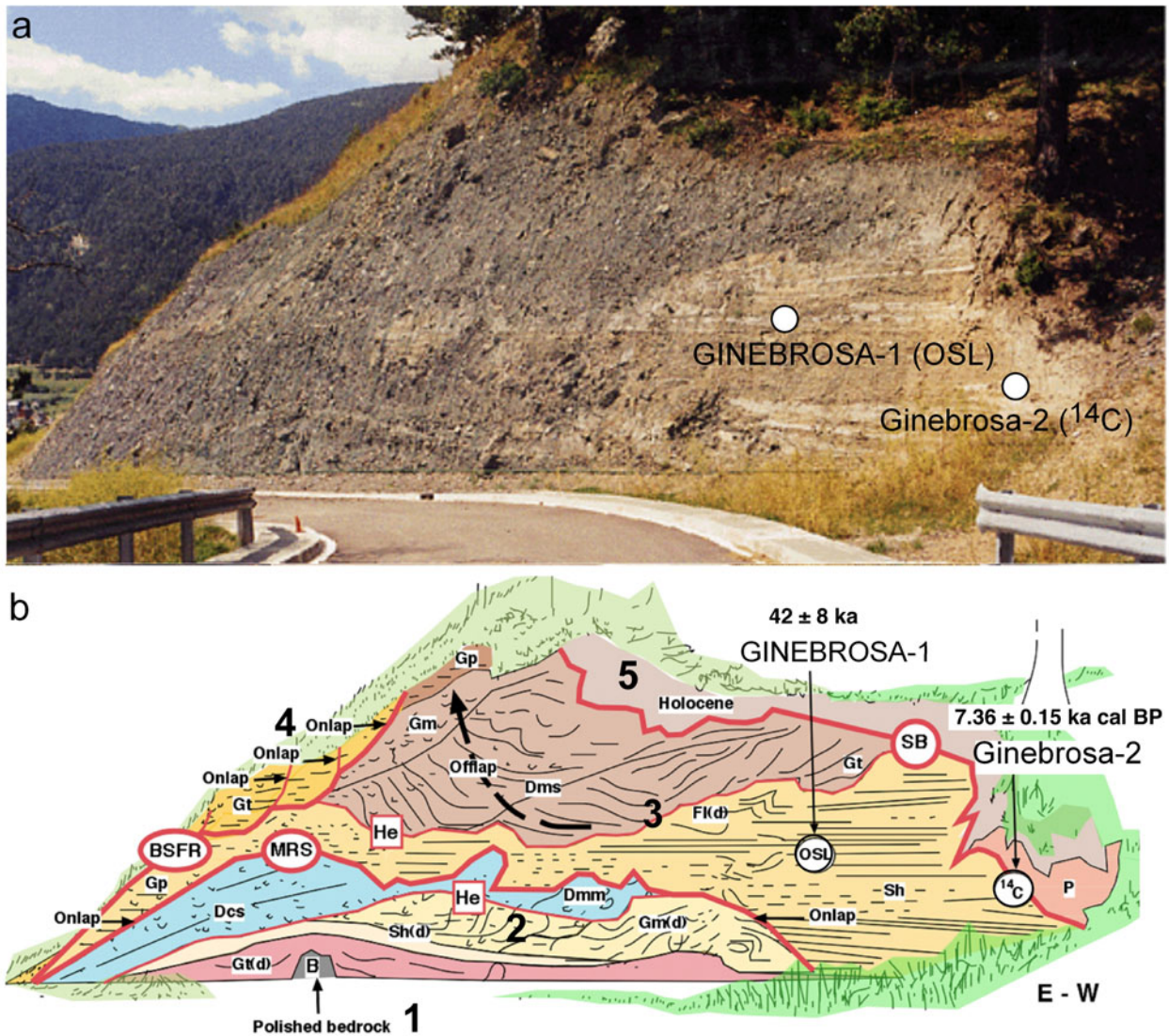
Figure 8. (a) Picture from the Ginebrosa outcrop (60 m long, 15 m high), showing the location of the samples. (b) Sedimentary units: 1, polished bedrock; 2, glacial unit; 3, main infill sequence; 4, final sedimentary stage; 5, recent colluvium and soil. Sedimentary facies identification: Dms: diamicton, matrix-supported, stratified; Dmm: diamicton, matrix-supported, massive; Dcs: diamicton, clast supported, stratified; Gm: massive or crudely bedded gravels, imbrication; Gm(d): deformed Gm; Gt: stratified gravels, trough crossbedding, minor channel fills; Gt(d): deformed Gt; Gp: stratified gravels, planar crossbedding; Sh: sand and pebbly sand, horizontal lamination; Sh(d): deformed Sh; Fl(d): deformed laminated fines (sands–silts and clays); P: pedogenic features, soils. Sequence stratigraphy surfaces and geometric relationships: arrows: offlap and onlap contacts; He: erosive surface; MRS: maximum regressive surface; BSFR: the basal surface of forced regression; SB: sequence boundary. Locations of the ^{14}C dating (GINEBROSA-2) and optically stimulated luminescence (OSL; GINEBROSA-1) samples as labelled.

older than 200–180 ka (Table 1); both levels may correlate with Calvet's T4 terrace (Calvet, 1998). Calvet's T3 terrace is 3–4 m thick and consists of sand lenses within gravels and cobbles. Cryoturbed colluvium deposits are connected to this terrace in the upstream area and suggest a cold context affecting this T3 glacis (Calvet, 1998). The age obtained for UR-1 (Fig. 4, 103 ± 13 ka) constrains the T3 terrace.

Near the Segre–Valira confluence (Fig. 1, sector 3), Turu and Peña-Monné (2006) correlated the Adrall deposits (ADRALL-3 and ADRALL-4; Table 1) and the Cal Tolse glaciofluvial sequence (LUM-27; Fig. 12) based on their similar states of weathering. Moreover, the ADRALL-3 and ADRALL-4 samples may come from a distal terrace (Fig. 14) of the Cal Tolse outwash when the Valira glacier front remained upstream at Sant Julià de Lòria (Llumeneres end-moraine till; Turu and Peña-Monné, 2006; Fig. 12). The recurrence of the main ice front in Sant Julià de Lòria was able to build several terminal complexes (Fig. 12); similarly, the tributary glacier was able to produce kame terraces in Segudet (Fig. 7), at both PGC (alpine Riss glaciation) and the LGC (alpine Würm glaciation). The Segudet kame complex, comprising the Cal Tolse terminal complex and the Adrall terrace (ADRALL-3 and ADRALL-4 samples; Tables 1 and 2), belongs to the Riss alpine glaciation (PGC). However, the glaciofluvial terraces are from the ADRALL-1 and ADRALL-2 samples (Table 2) and, therefore older than 180 ka (ADRALL-4; Table 1). Close to the Valira–Segre confluence, the glaciofluvial terrace represented by sample ADRALL-2 correlates with the Tossal Bordar far-flung moraine (Turu and Peña-Monné, 2006; Fig. 1, sector 3) located +100 m arb. The intense weathering of the ADRALL-2 glaciofluvial terrace (Poch et al., 2013) advocates for an age older than the MIS 6 glaciation, but it is unfortunately still undated.
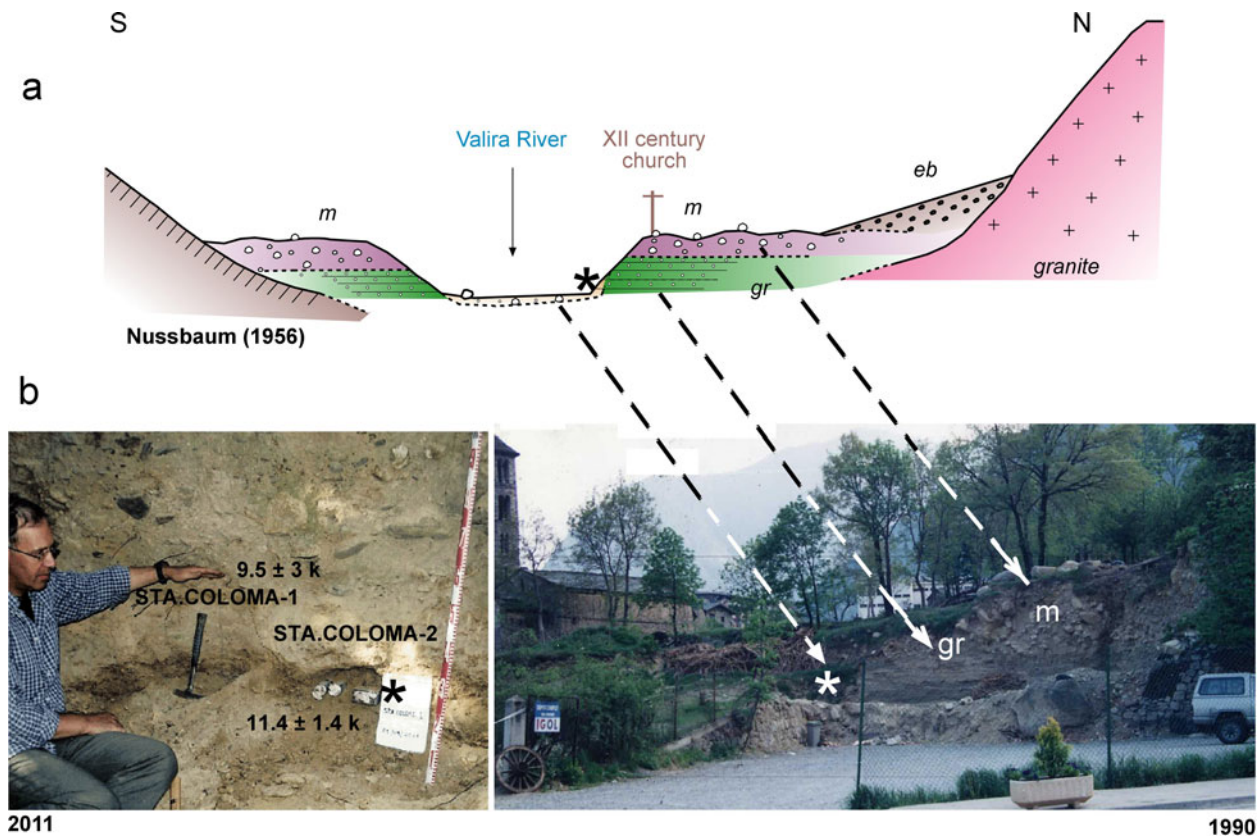
Figure 9. (a) Interpretative section from Nussbaum (1956) at Santa Coloma (Andorra); m, moraine, gr, gravels, eb, boulders. (b) Arrows indicate sedimentary units from Nussbaum (1956) and in the 1990s outcrop. Two samples were collected from the same layer and position of the Santa Coloma fluvial terrace.

The western area

The Sant Mamés melt-out till (73.9 ± 4.5 ka; VILALLER-2; Table 1) provides information about the upper age limit for the LMIE phase, belonging to the end of the MIS 5a–MIS 4 interval. The distribution of erratic boulders over the slopes in Vilaller (Mey, 1965; Vilaplana, 1983a, 1983b; Rodés, 2008), as well as a few remains of kame terraces close to the Noguera de Tor confluence, indicates that the tributary glacier joined the main glacier (Noguera Ribagorçana) during the LMIE and the resulting glacial front finished at the village of Pont the Suert. Unfortunately, no end moraine could be identified there. However, the former glacial front should be close to its outwash, which is the glaciofluvial terrace located south of Pont de Suert (Fig. 2).

Once the Noguera Ribagorçana glacier retreated from the LMIE position, it emplaced the southernmost till identified from outcrops in the study area that was 2 km south of Vilaller (Fig. 2); this is the Sant Antoni till (∼940 m) (Vilaplana, 1983a, 1983b; Bordonau, 1992; Pallàs et al., 2006). Located ∼15 m above the Noguera Ribagorçana riverbed, it includes abundant rounded to subangular granodiorite boulders ≈1 m in diameter (Pallàs et al., 2006 and references therein). However, the absolute age of the Sant Antoni till is still unknown.

The glaciofluvial deposits of Sant Mamés (Vilaplana, 1983a; Bordonau et al., 1989; Bordonau, 1992; Pallàs et al., 2006; Fig. 2) correspond to the end of the infilling of the Seminari de Vilaller overdeepened trough (Fig. 5). Three AMS ^{14}C ages were obtained in the glaciolacustrine infill (Bordonau, 1992; Fig. 5)

just behind the Seminari de Vilaller frontal moraine (Gif-8638 at ∼26.15 m depth; Gif-8639 at ∼26.00 m depth; and Gif-8640 at ∼21.95 m depth). Their ages were as follows: Gif-8638 is 38.684–31.891 ka cal BP ($δ^{13}$C = −23.55‰); Gif-8639 is 25.201–23.372 ka cal BP ($δ^{13}$C = −24.02‰); and Gif-8640 is 39.149–33.449 ka cal BP ($δ^{13}$C = −23.45‰). The age reversal between samples (Fig. 5e) left the chronology of the moraine buildup as an unsolved question (Bordonau, 1992). Nevertheless, two moraine ridges flank the valleys at this point, the Llestui within the Llauset tributary and the Artigallonga (1715 m), which is a lateral moraine complex (Fig. 2) at +600 m (Bordonau, 1992), where Pallàs et al. (2006) obtained ^{10}Be CRE ages from glacial boulders. The updated CRE ages from Tinabre and Artigallonga can be found in Supplementary Material 7: 26.9 ± 6.2 ka (TIN01), 23.4 ± 3.4 ka (ART02), and 20.8 ± 5.1 ka (ART03) (Fig. 2); they are similar to those reported by Delmas et al. (2021b). However, these ages are compatible with those from Lake Llauset (25.886–24.467 ka b2k; Vilaplana, 1983a), which was then ice-free (Montserrat-Martí, 1985), a circumstance not reported by Delmas et al. (2021b). Therefore, the main Noguera Ribagorçana glacial system penetrated the Llauset valley and formed a paleolake at Llestui (Fig. 2) at 26.9 ± 6.2 ka (TIN01; 1301 m) and extended beyond Vilaller, not in the Seminari de Vilaller (993 m) as Pallàs et al. (2006) suggested. Thus, the age of the Seminari de Vilaller frontal moraine complex (Fig. 5e) is probably equivalent to the youngest age of the Artigallonga lateral moraine complex (Fig. 2), and that is 20.8 ± 5.1 ka (ART03). Moreover, the infill of the valley bottom behind the Seminari de Vilaller (Fig. 5e) should be older than the age of Tinabre
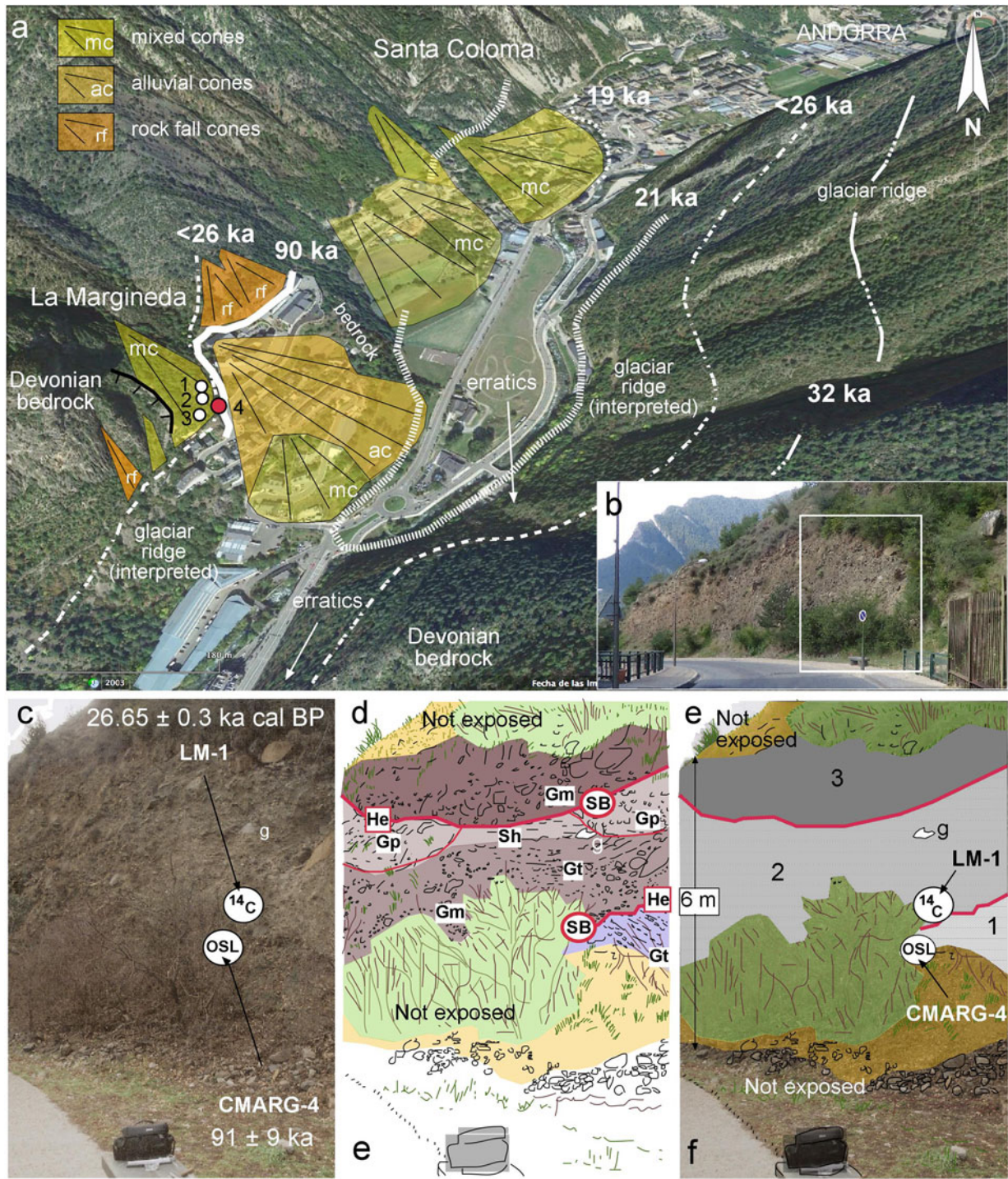
Figure 10. (a) La Margineda and Santa Coloma geomorphology, overprinted on an image from Google Earth. Cited sites are indicated with the location of the dated samples: 1, LM; 2, LM-2a; 3, LM-2b; 4, CMARG-4. The lines mark the limits of the Valira glacier at different dates. (b) A general overview of deposits on top of the hill. The rectangular area shows the consolidated colluviums in parts c to e. (c) A closer look at the consolidated colluvium. (d) Sedimentary facies: Gm: massive or crudely bedded gravels, imbrication; Gt: stratified gravels, trough crossbedding, minor channel fills; Gp: stratified gravels, with planar crossbedding; Sh: sand and pebbly sand, with horizontal lamination. The sequence boundaries (SB) between units are erosive (He). (e) La Margineda sedimentary units: unit 1: gravels and sands having coarse crossbedding; units 2 and 3: fining-upward sequences of colluvium; g: granite. The locations of the samples for optically stimulated luminescence (OSL) and ^{14}C dating are represented in parts c and e.

(TIN01), returning a minimum age of 39.149–31.891 ka cal BP (Gif-8638 and Gif-8640); thus, the age of Gif-8639 (Fig. 5e) must be rejected. It should be noted that δ^{13}C from Gif-8636 is slightly depleted compared to the other two, which could imply

the inclusion of younger bulk carbon within the sample, not inactive carbon (cf. Pallàs et al., 2006), giving an older age. If not amended, it is usual that contamination occurs during the borehole extractive procedure (Turu et al., 2018).
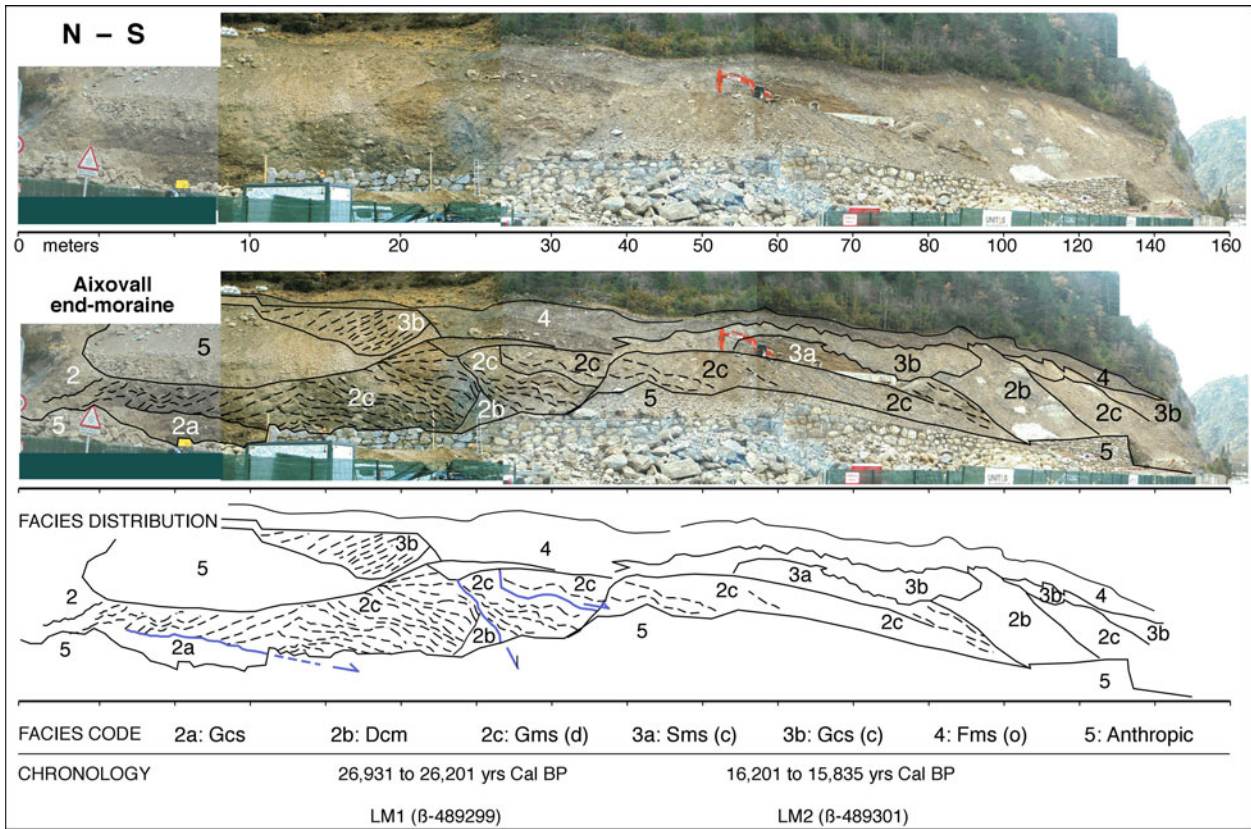
Figure 11. The Aixovall LGM end moraine (937 m asl) and stratigraphy from La Margineda at Aixovall. Facies 2a: glaciofluvial imbricate gravels; facies 2b: supra-glacial till, including boulders of local (calcschists) and allochthonous (black slates) lithology; facies 2c: tilted bedding of glaciofluvial gravels mixed with coarse colluvium within thrusted blocks induced by glaciotectonics; facies 3a: stratified slope deposits, matrix-supported; facies 3b: cemented grèzes litées; facies 4: organic colluvium; facies 5: masonry, artificial slopes, and sections disturbed by excavation.
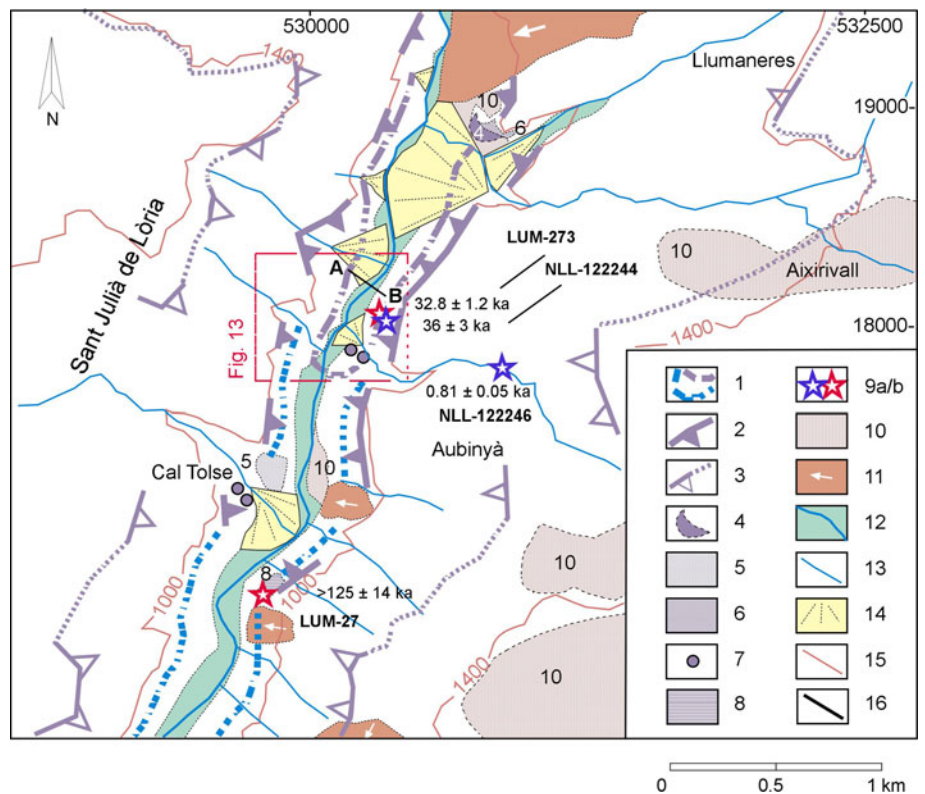
Figure 12. Geomorphological sketch map from the Sant Julià de Lòria area: 1, the younger than MIS 4 glacial fronts at Sant Julià de Lòria and Bastida de Ponts glacial front; 2, glacier ridge previous to 180 ka after the Cal Tolse till; 3, the MIS 4 LMIE glacial ridges of Pont Trencat glacial front; 4, front-lateral till deposits from the Cal Tolse–Adrall 4 outwash (~180 ka); 5, hump (glacial); 6, undifferentiated till; 7, erratic boulders; 8, glaciofluvial deposits recorded to (4); 9, available dates (red: thermoluminescence [TL] sample; blue: optically stimulated luminescence [OSL] sample); 10, colluvium; 11, landslide; 12, modern riverbed deposits; 13, stream; 14, alluvial fan; 15, topographic contour lines (meters above sea level); 16. Profile A-B interpreted in Fig. 13d.
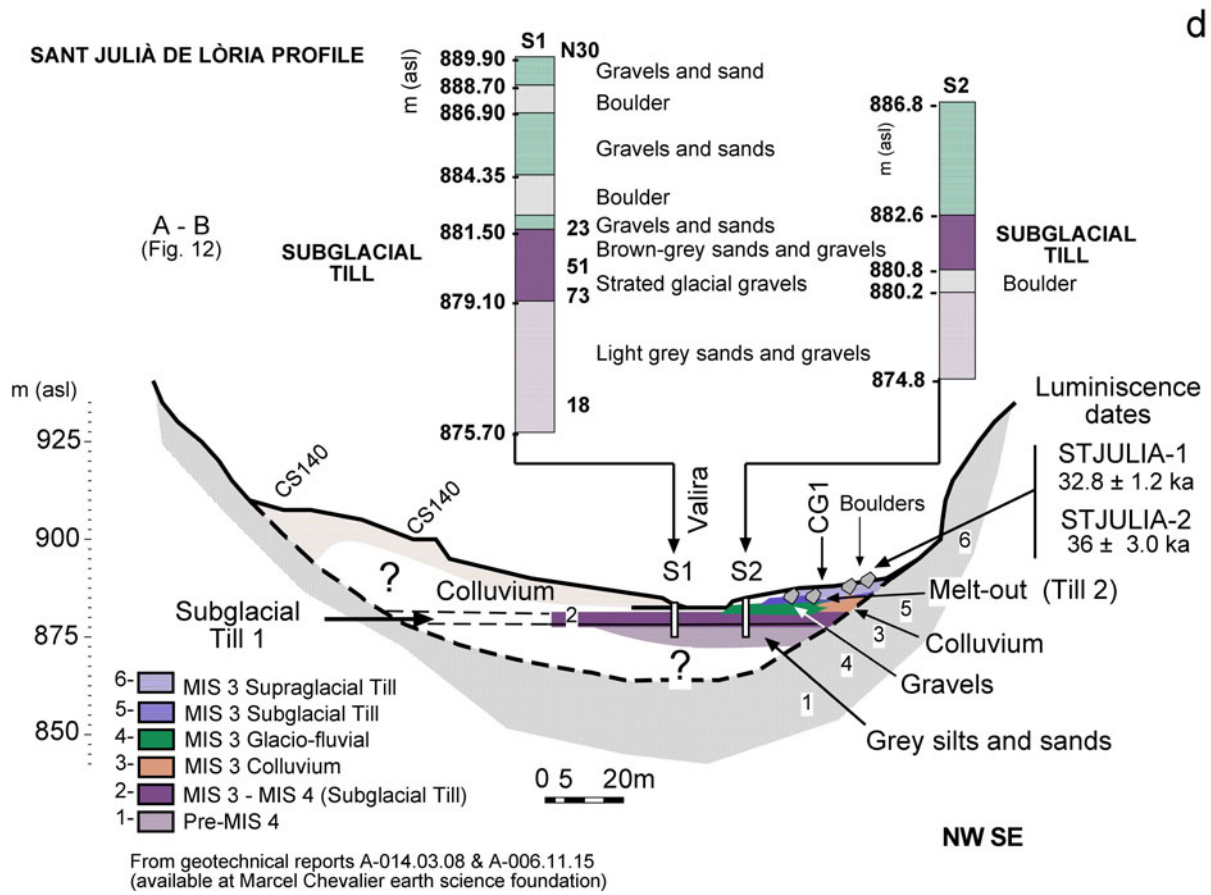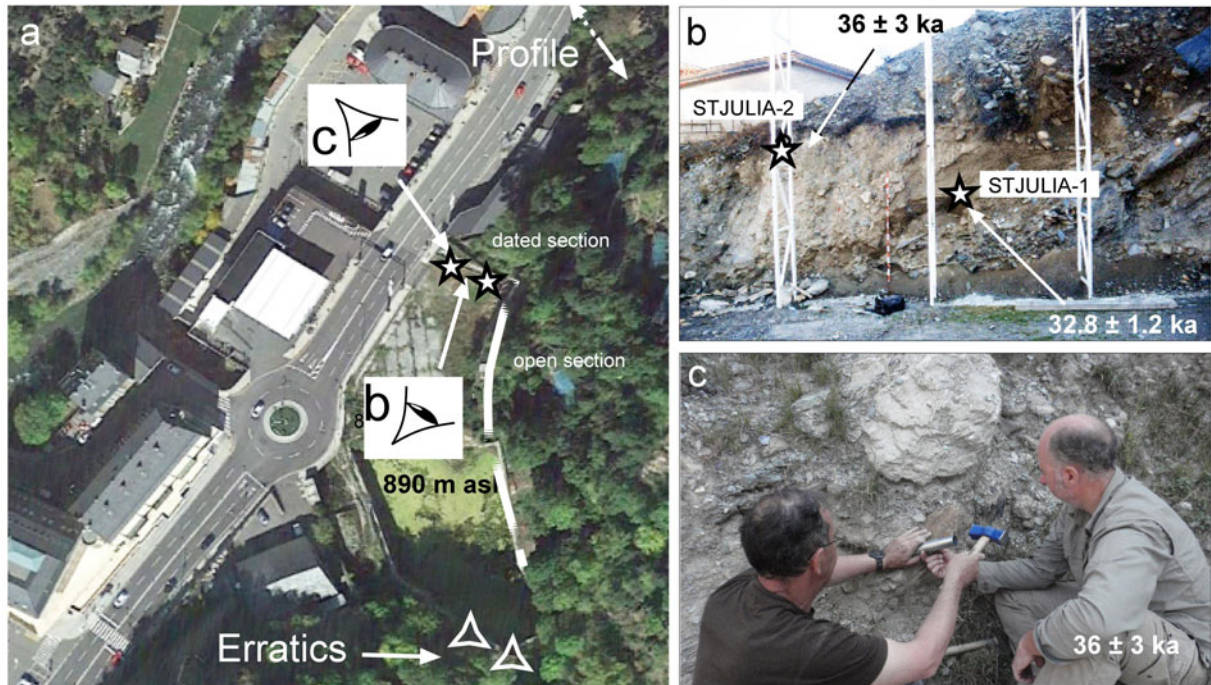
Figure 13. (a) Google Earth image from the south Sant Julià de Lòria area. Point of view (eye symbol) of extensive open-pit excavation and sedimentary descriptions. The position of the dated section is labelled. (b and c) Pictures of the outcrop with the location of the sample ST JULIA-1 from cross-stratified sands (March 2006) and ST JULIA-2 from laminated sands on a melt-out (taken September 2011). (d) Stratigraphy of the Sant Julià de Lòria valley floor. The dated supraglacial system (samples STJULIA-1 and STJULIA-2) includes colluvium facies (3), glaciofluvial gravels (4), and melt-out till (5).
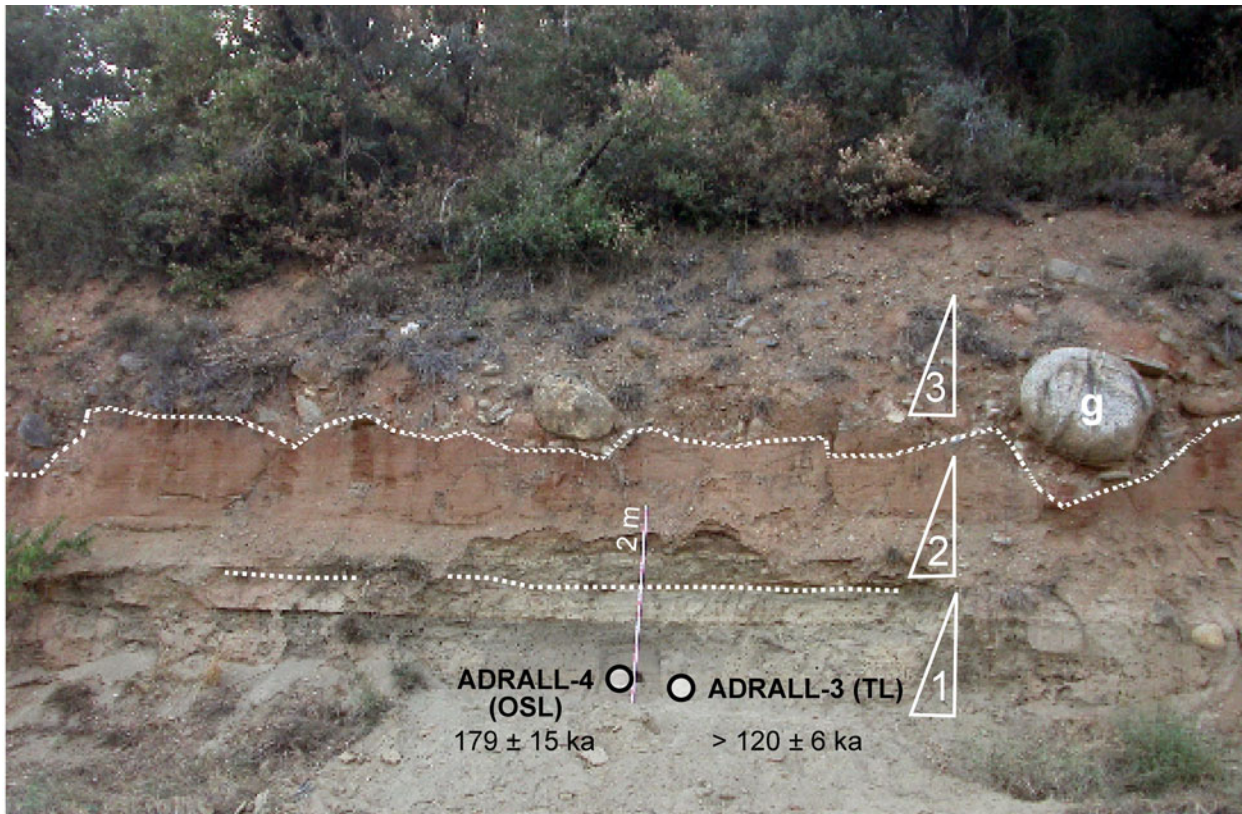
Figure 14. The upper division of the Segre-Valira glaciofluvial T5 terrace at the Adrall site. Location of the ADRALL-3 (thermoluminescence [TL]) and ADRALL-4 (optically stimulated luminescence [OSL]). The lower part of the exposure contains fine to coarse sands, while the upper portion comprises rounded boulders and imbricated cobbles and pebbles (g: granite boulder).

The eastern area

In the Valira valley, the CMARG-4 (91 ± 9 ka; Table 1) sample gave an age within MIS 5c for the Valira glacier terminal complex at La Margineda, which is possibly equivalent to the Ur glaciofluvial terrace (103 ± 13 ka, MIS 5c; UR-1; Table 1). The early Würm (MIS 5c) glacial front of La Margineda (Fig. 10) is 4.6 km upstream from the Cal Tolse Rissian terminal complex (Fig. 3); thus, in Cerdagne, the corresponding T3 end moraine would have been located upstream of the Ur locality and would
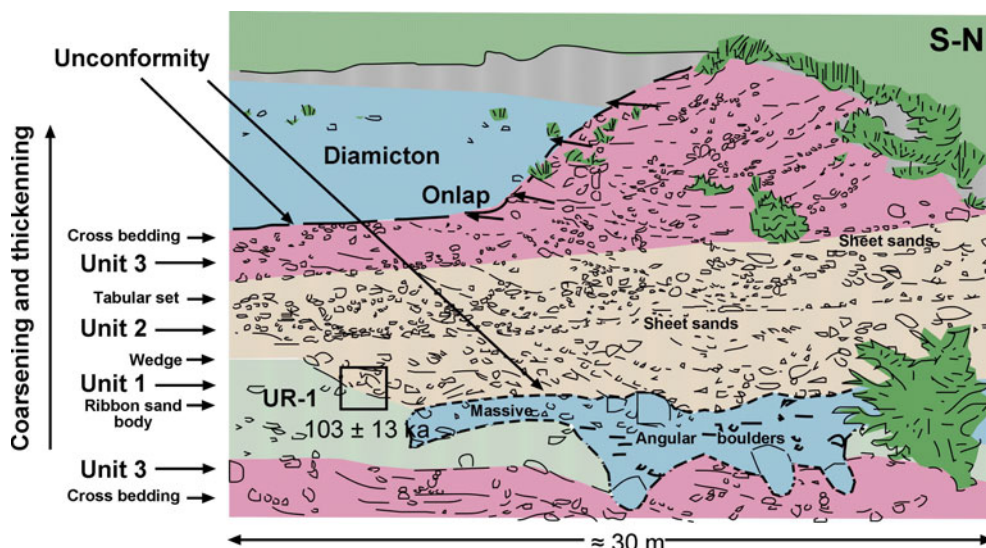

Figure 15. Drawing showing an interdigitation of glaciofluvial channel deposits (units 1, 2, 4, and 5) with tills (units 3 and 6). Original photography from Calvet et al. (2011a). The glaciofluvial unit was sampled (UR-1), indicating its correlative location. (Colours are only for guidance.)
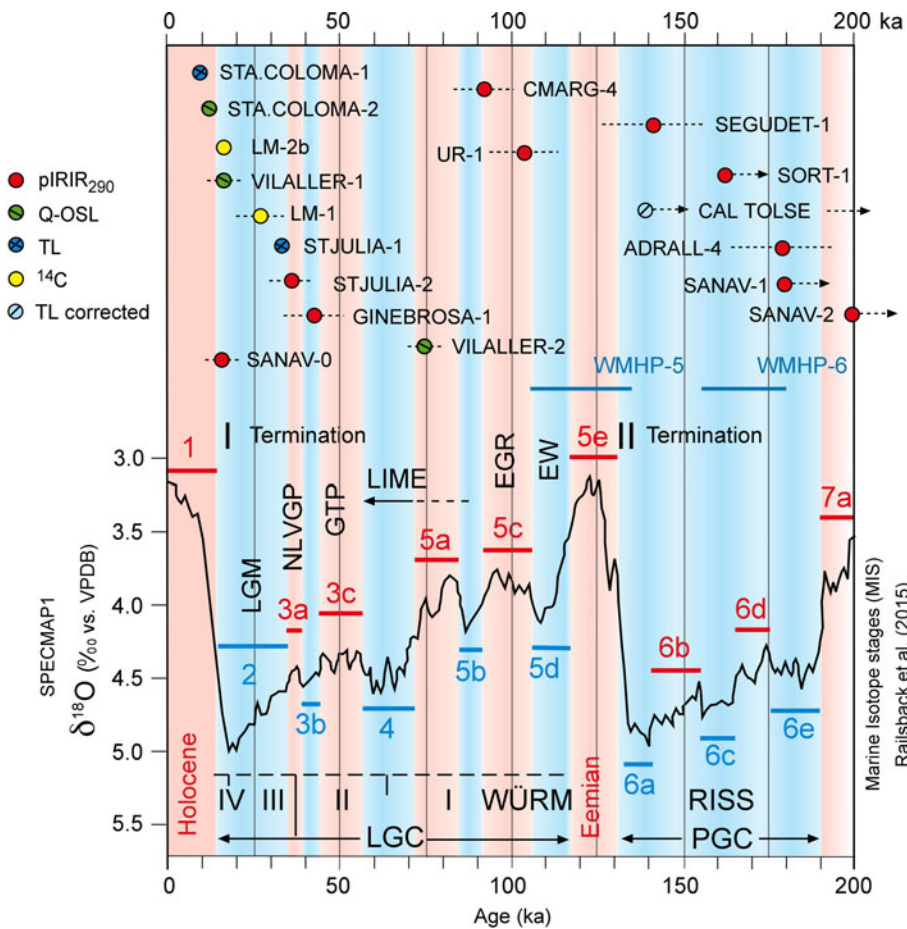
Figure 16. Thermoluminescence (TL), quartz optically stimulated luminescence (Qtz-OSL), pIRIR290, and ^{14}C ages plotted over the Specmap1 curve and the marine isotope stages (MIS) for the last 200 ka (modified from Railsback et al., 2015; Martinson et al., 1987). SANAV-0 may indicate the pIRIR290 offset in the uppermost River Segre. Penultimate glacial cycle (PGC) or Riss, the last interglacial (Eemian), the last glacial cycle (LGC) or Würm and subdivisions (I, II, III, IV; based on Renault-Miskovsky and Girard, 1998). Terminations I and II indicated; as well, the Western Mediterranean Humid Periods (WMHP) 6 and 5. South-central eastern Pyrenean glacial phases: early Würm (EW), early glacial recession (EGR), last maximum ice extent (LIME), glaciers thinning period (GTP), no large valley glaciers period (NLVGP), and the global last glacial maximum (LGM) period.

have been surpassed by later glacial advances forming the M1 and M2 close-nested moraine complex (Barr and Lovell, 2014) of the River Querol (Pallàs et al., 2010; Fig. 4).

From the tributary valley of Arinsal (NW Andorra), four sedimentary episodes are distinguished in the Ginebrosa kame complex (Fig. 8), documenting glacial evolution during mid-MIS 3: (1) deposition of lodgement till at the beginning of MIS 3 or earlier; (2) a mid-MIS 3 glacial thinning and stabilisation phase (42 ± 8 ka; GINEBROSA-1; Table 1) with deposition of rhythmites and a predominance of fine sands; (3) glacial advance and deformation of previous deposits, shearing, and supraglacial till deposition; (4) rapid glacial retreat during MIS 3 affecting also the main glacier (Turu et al., 2017).

The main glacial front retreated back to Sant Julià de Lòria (Fig. 13), and there was buildup of a new terminal complex between 39 and 31 ka (STJULIA-1 and STJULIA-2; Tables 1 and 2). However, the Santa Coloma fluvial terrace from the Valira River is much younger, dating from MIS 1 (terrace T9 of Peña-Monné et al. [2011]). The MIS 2 end moraine in Santa Coloma (Nussbaum, 1956; Turu et al., 2007, 2017) had been partially eroded or overlapped by later outwash.

DISCUSSION

We found some key deposits from the Segre River tributaries that are beyond the range of the K-feldspar OSL dating method (Fig. 16), always weathered, and mainly located beyond the limits of the maximum Würmian glaciation (LGC) (Turu and

Peña-Monné, 2006; Lewis et al., 2009; Jalut et al., 2010; García-Ruiz et al., 2013; Oliva et al., 2019). An example of this is in Cerdagne, where moraine M3 was assigned to the middle Pleistocene (Calvet et al., 2013), and we now correlate it with the older than 200 ka Sanavastre terrace (Fig. 17a, T4).

No dates were found from the last interglacial (MIS 5e, the Eemian interglacial) (Fig. 16). Very few dates were also found by Lewis et al. (2009) in fluvial and glaciofluvial terraces from the SW Pyrenees that belong to the Eemian interglacial. However, deposits yielding MIS 6 ages are much more common. We can highlight the following examples within the Western Mediterranean Humid Period 6 and 5 (WMHP, Camuera et al., 2022): (1) the end moraine of Castiello de Jaca (171 ± 22 ka), a far-flung moraine from the Aragon glacier (García-Ruiz et al., 2011, 2013; Fig. 1); (2) the glaciofluvial terrace in the upper Gállego valley at Sabiñanigo-Alto (155 ± 24 ka; 156 ± 10 ka; Lewis et al., 2009; Fig. 1); (3) a terrace of the Cinca River (the westernmost tributary of the Segre) at Belver (171 ± 21; terrace Qt5, 180 ± 22; Lewis et al., 2009), all belonging the WMHP-6; (4) the terrace at Arén in the Noguera Ribagorçana valley (Qt13 terrace, 131 ± 7 ka; Peña-Monné et al., 2021); and (5) in the lower Segre (Ebro depression at Lleida; Fig. 1), or the MIS 6 ages obtained in the fluvial Qt2 terrace (+80 m) by Stange et al. (2013); belongs to the WMHP-5. From the northern slope of the Pyrenees, we highlight the Garonne (Fig. 1) terminal complex of La Serre (Fernandes et al., 2017), where an end-MIS 6 age from the WMHP-5 were reported by Fernandes et al. (2021) for the outermost end moraine (MIE; Fig. 17b), and later glacial advances built a

close-nested end moraine (Fig. 17b) ranging from >40 ka cal BP to MIS 2 around Lake Barbazan (Andrieu et al., 1988).

Deposits that are beyond the range of the Qtz-OSL dating method (>80 ka) are found beneath the LMIE glacial front limits and show weathering according to their ages (Rixhon, 2022). The best example in our area corresponds to the multi–glacial cycle nested moraine of La Margineda, where the early Würm end moraine (+65–75 m arb; 91 ± 9 ka, MIS 5b–5c; CMARG-4; Fig. 10e; Table 1) was surpassed by later glacial advances (Fig. 17c). In the NE Pyrenees (Niaux Cave, NE Pyrenees, 678 m; Fig. 1) an early Würm glacial progression has also been dated using U–Th methods (Bakalowicz et al., 1984), leading to the conclusion that the Ariège glacier was in the vicinity of the cave at ~95 ka, within the MIS 5d–5c interval (Sorriaux et al., 2016), 13 km upstream from the MIS 6 terminal complex (Delmas et al., 2011). The onset of the LGC was probably synchronous on both sides of the Pyrenees because a similar age comes from the glaciofluvial terrace at Ur (Fig. 1, sector 4).

Deposits that are within the range of the Qtz-OSL dating method (<80 ka) belong to the LMIE or are found upstream from the LMIE glacial front limits, always weakly weathered. Our best example is the Sant Mamés melt-out till (Fig. 17d) from the MIS 5a–MIS 4 interval. The Sant Mamés melt-out till (73.9 ± 4.5 ka; VILALLER-2; Fig. 5, Table 1) can be correlated with the M2 end moraine from the Aragon glacier at Castiello de Jaca (SW Pyrenees; García-Ruiz et al., 2011, 2013; Fig. 1). The Sant Mamés diamicton also correlates with the Sant Marcial (Fig. 1) glaciofluvial deposits of the Cinca glacier (SW Pyrenees; 76 ± 13 ka; Lewis et al., 2009). Glaciers must then have retreated from their maximum positions, as a glaciofluvial terrace at Castiello (Fig. 1) gave an OSL age of 68 ± 7 ka, indicating a less extensive glacial front than during the LMIE (moraine m2, 51 ± 4.5 ka; García-Ruiz et al., 2011, 2013). In the upper Cinca valley, OSL dates from glaciofluvial terraces gave ages of 63 ± 6 ka and 49.5 ± 3.9 ka (Salinas de Sin; Supplementary Material 8). To the east, the Sant Mamés melt-out till (Fig. 5) correlates with the oldest available exposure ages from the outermost Malniu moraine: 76.5 ± 7.1 ka, [10]Be (GS-20), and 49.2 ± 4.5 ka, [10]Be (GS-14), both dates falling within the MIS 5a–MIS 4 interval (Fig. 1, sector 4). However, Tomkins et al. (2018, 2021) suggested that the LMIE in the Pyrenees was at 40.9 ± 1.1 ka (MIS 3) and coincided with the Hengelo interstadial. It seems unlikely that the LMIE coincided with the French archaeological Würm II–Würm III subdivision (Renault-Miskovsky and Girard, 1998). Evidence from glaciated mountains and ice sheets worldwide (Hughes et al., 2013) does not indicate more significant glacial advances in MIS 3 than during MIS 2 or MIS 4 (Allard et al., 2021). The constrained LMIE age obtained by Tomkins et al. (2018, 2021) is probably beyond the limits of their method (Moses et al., 2014).

Unexpectedly, some of the deposits within the MIS 3 range of the AMS ^{14}C-dating method (≈45 ka) are found in an inner position within the glacial valley far from the LMIE and LGM glacial front limits. We refer to these deposits as resulting from an ice or glacial thinning recession within the LGC and corresponding to the relevant palaeoenvironmental evidence from the northern foothills of the Pyrenees, which were occupied by the Neanderthals during the Châtelperronian, spanning from ca. 44.5 ka cal yr BP to 38.5 ka cal yr BP (Bricker, 2014). The archaeological site of Tambourets is only a few kilometres beyond Barbazan (Fig. 1), where a close-nested end moraine from the Garonne glacier is located (Andrieu et al., 1988; Fernandes

et al., 2021). Bricker (2014) described archaeological remains within loess-type deposits from the beginning of Heinrich Event 4 (GS-10; Rasmussen et al., 2014). However, a brief episode of milder climate (Bricker, 2014) during GI-9 (Rasmussen et al., 2014) preceded the resumption of severe cold and dry conditions during stadial GS-9 (Rasmussen et al., 2014). We attempt to correlate this to the available sedimentary record from the southern slope of the Pyrenees as follows:

1. The highest flooding level in Ginebrosa (Fig. 8, unit 3), recorded after 42 ± 8 ka, may be related to an increase in ice-damming that we assign to stadial GS-11 (42,240–41,460 b2k; Rasmussen et al., 2014). Unit 4 (Fig. 8) indicates that the ice tongue thinned rapidly, probably during GI-10 (41,460–40,800 b2k; Rasmussen et al., 2014).

2. The Sia (SW Pyrenees; Serrano et al., 2011) and Gavin lateral moraine complex (Fig. 1) was built (Fig. 17e) by the Gállego glacier at 42 ± 7 ka (49–35 ka; X1596; Supplementary Material 8). Guerrero et al. (2018) reported a major ice-thinning phase of the Gállego glacier ~41.53 ± 3.95 ka (OSL) from the Sextas earthflow (1630 m asl, SW Pyrenees; Fig. 1). The erstwhile Ara glacier thinned shortly after unblocking the Linas de Broto ice-dammed palaeolake (Sancho et al., 2018; Bartolomé et al., 2021).

Daura et al. (2013) indicated a significantly arid climate during GS-9 in NE Iberia, matching the cold and dry climate reported at Tambourets by Bricker (2014) and the recession mentioned above of the Gállego, Ara, and Valira glaciers. At the end of MIS 3 (ca. 39.7–34.2 ka cal BP; Turu et al., 2017), the retreat of the Valira d'Orient glacier at Canillo (NE Andorra; 1530 m asl; Fig. 1) may have been responsible for an early triggering of the El Forn landslide (Corominas et al., 2015). Between GI-10 and GI-7 (Rasmussen et al., 2014), glaciers receded synchronously at both extremities of the southern slopes of the Pyrenees.

On the northern slopes of the Pyrenees, the glacial recession has also been documented at Lourdes (Mardones and Jalut, 1983) and Barbazan (Andrieu et al., 1988). However, during the MIS 3–2 transition, the Garonne glacier again spread across Barbazan (36.2– 31.3 ka b2k, 29.5 −1.182/+1.38 ka BP; Andrieu, 1991). On the southern slope of the Pyrenees, the late MIS 3 terminal complex of Sant Julià de Lòria (STJULIA-2 and STJULIA-1; Tables 1 and 2) correlates with the Senegüé (Fig. 17e) glacial phase in the upper Gállego (Lewis et al., 2009).

In La Margineda (Fig. 10c), a set of colluvia (26.65 ± 0.3 ka cal BP; LM1; Table 3) were consolidated by the regrowth of the Andorra glacier when it reached its LGM positions 1 km downstream of La Margineda (Fig. 11). An early LGM (Clark et al., 2009) was registered in the southern slope of the Pyrenees by the buildup of the Tinabre lateral moraine (Fig. 2), and it is also evident from the buildup of the innermost lateral moraine ridge from Gavin (Fig. 17e) at 28 ± 3 ka (sample X1595; Supplementary Material 8). However, the LGM period (Clark et al., 2009) was quite unstable in the southern slope of the Pyrenees because the glacial recession and regrowth produced reworking and deformation of the sediments in the La Massana palaeolake (Turu et al., 2017); slope instability in Andorra (VB05-30.2, 26.010–25.828 ka b2k; 21.52 ± 0.070 ka BP; Planas and Torrebadella, 2022); moraine ridge duplication (Tomkins et al., 2021), as in the case of the Artigallonga moraines (Fig. 2); and the recurrence of ice-damming at Llestui (Fig. 2). Evidence from the late LGM period was also reported upstream
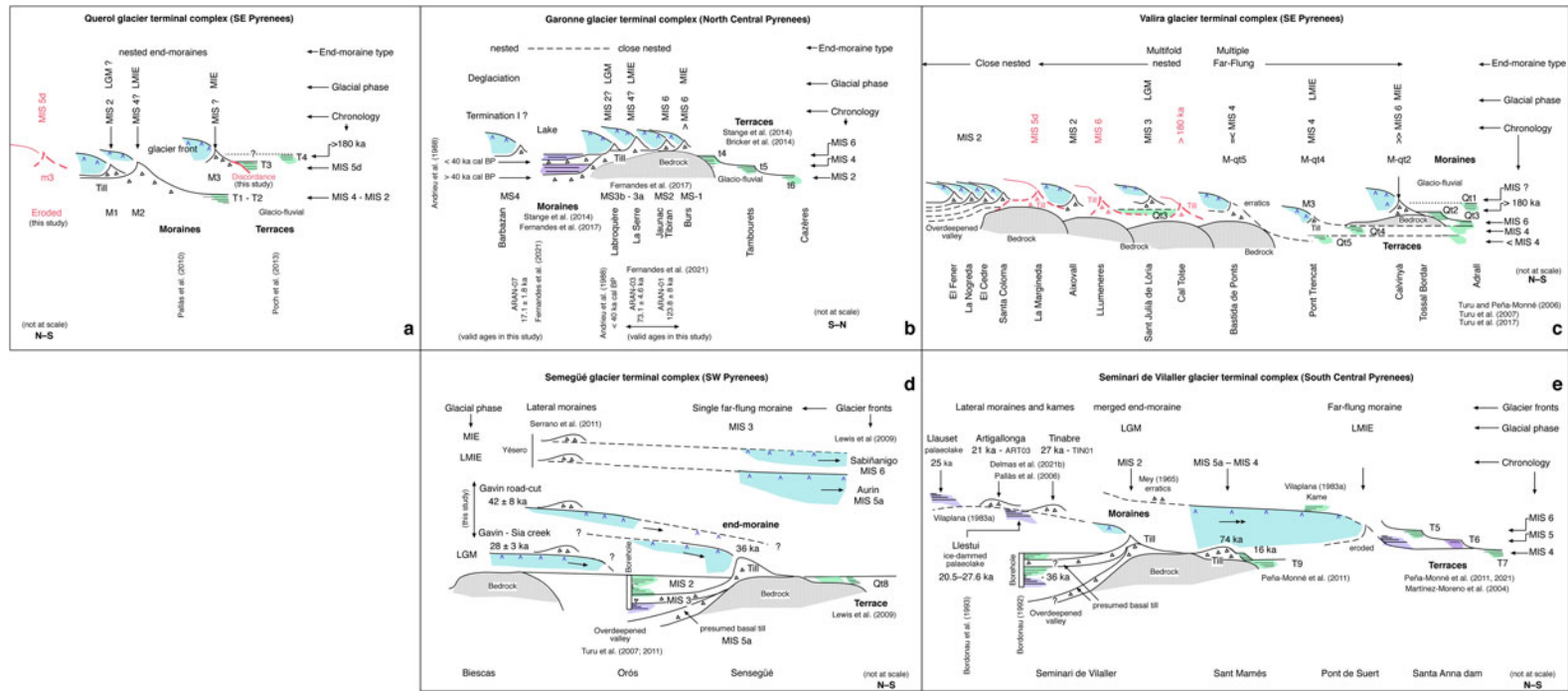
Figure 17. Classification of the glacial terminal complexes from the south-central and southeastern slope of the Pyrenees, including, for comparison, a case from the SW Pyrenees and the north-central slope of the mountain range. (a) Querol terminal complex formed by nested end moraines (Pallàs et al., 2010) and the related glaciofluvial system of terraces (Poch et al., 2013). Terrace T3 onlap, the oldest end-moraine M3 correlated with the oldest glaciofluvial level (T4). (b) The Garonne terminal complex, formed by close-nested and nested end moraines (Stange et al. (2014) and Fernandes et al. (2017)). The oldest ages from the outer end moraine are from MIS 6; however, younger ages were also reported by Fernandes et al. (2021) in this terminal complex that can be correlated with the glaciofluvial terraces (Bricker et al. 2014) and the chronology of lake Barbazan (Andrieu et al., 1988) and their surrounding end moraines. (c) The Valira terminal complex is the most diverse case (Turu and Peña-Monné, 2006). The Valira glacier partially eroded MIS 6 end moraines during the LGC, building multifold-nested and close-nested moraines (Turu et al., 2017). Beyond, multiple far-flung end moraines correlated with the Segre-Valira staircase system of glaciofluvial terraces (Turu et al., 2007). (d) The Gállego terminal complex centred around Senegüé (Turu et al., 2007), the best-preserved end moraine (Lewis et al., 2009). Unpublished dates (Supplementary Material) from the Gavin lateral moraine ridges (Serrano et al., 2011) allow the reconstruction of glacial evolution behind and beyond Senegüé (Turu et al., 2011). (e) The Ribagorçana terminal complex around its best-preserved end moraine (Mey, 1965; Vilaplana 1983a; Bordonau 1992), the Seminari de Vilaller (Bordonau et al. 1993; Pallàs et al. 2006). Calibrated and recalculated dates (this work) from the lateral moraine ridges and kames behind the end moraine (Delmas et al. 2021b). Glacial front in Pont de Suert (reconstructed). The ages of the glaciofluvial deposits (Peña-Monné et al. 2011) are from the archaeological data of Martínez-Moreno et al. (2004) and Peña-Monné et al. (2021).

of Sextas (Fig. 1) by Gonzalez-Sampériz et al. (2006), and for the Santa Coloma end moraine (Turu et al., 2007, 2017; Fig. 9).

Glacial tongue asymmetries within the LGM period (22.25 ± 4.25 ka; Clark et al., 2009) and between the LMIE and LGM phases occur between Pyrenean valleys; only in Cerdagne does the close-nested end moraine (Fig. 4, M1 and M2) from the Querol glacier seem to span from MIS 4 (Delmas et al., 2008; Calvet et al., 2011a) to MIS 2 (Pallàs et al., 2010), highlighting that the LMIE and the LGM had similar glacial extents in the southeasternmost slope of the Pyrenees (Fig. 17a). However, this is not seen in the south-central Pyrenees, where an LGM end moraine (Fig. 17d) in the Seminari de Vilaller is far from the LMIE limits at Pont de Suert (Fig. 2). Subsequently, the final glacial retreat occurred toward the end of the last termination. In the Noguera Ribagorçana (Fig. 17d), it is represented by the end of the infilling of the overdeepened trough at around 15.7 ± 1.2 ka (VILALLER-1; Table 1), when the local glacial fronts were located at Santet and Bissiberri (Pallàs et al., 2006; Fig. 2; [10]Be exposure ages recalculated, Supplementary Material 7). However, in the neighboring eastern valley, the Noguera de Tor (Fig. 2), the disappearance of cirque glaciers took place at 16.4–16.0 cal ka BP (Copons and Bordonau, 1996), and only at ≈2200 m did small glaciers survive in this valley until 12.05 ± 0.4 ka (Tomkins et al., 2021). In the Valira d'Orient valley (Fig. 3), the glacial thickness was less than 250 m at 15.3 ± 1.1 ka, the timing of the triggering of the Encampadana *sackung* (1625 m asl; McCalpin and Corominas, 2019; Fig. 1). The retreat of the Valira d'Orient glacier from Canillo preceded the second triggering of the Forn landslide at 13.144 ± 0.175 ka cal BP (Turu and Planas, 2005; Fig. 1, sector 3) and the blockage of the Valira d'Orient valley at Canillo (1530 m asl).

CONCLUSIONS

We distinguish between two types of terminal complexes, those in which there is at least one far-flung end moraine (Fig. 17d and e) and those in which there is not (Fig. 17b); however, both include nested moraines and/or a close-nested end-moraine complex (Fig. 17a and b). Close-nested end-moraine complexes encompass at least two glacial cycles: the LGC and the penultimate glacial cycle (Fig. 17b), and these moraines could be termed "multiple nested moraines" (Fig. 17c). Of note, the end moraines from the penultimate glacial cycle (MIS 6) are common in the whole range of the Pyrenees and were formed during the Western Mediterranean Humid Period 6 and 5.

The starting point for cooling in the LGC was generally at ∼97 −15/+19 ka (Niaux, UR-1; Fig. 16), in MIS 5d, synchronous on both sides of the Pyrenees, and we refer to the early Würm (Fig. 16, EW). However, the MIS 5d Valira glacier front (Fig. 17c) was far from the LMIE far-flung moraine, and this could also be the case for other glaciated valleys in the Pyrenees (Fig. 17a).

The LMIE advance occurred at the beginning of MIS 4 (Fig. 16, VILALLER-2), after an early glacial recession (Fig. 16, EGR) after/following MIS 5d. Literature consultation enabled us to compare the glaciated Noguera Ribagorça valley with its neighbouring valleys, allowing the identification of a significant glacial thinning (Fig. 16, GTP) and glacial front retreat during the second half of MIS 3 (Fig. 16, GINEBROSA-1), during which glaciers thinned and receded or almost disappeared (no large valley glacial period [NLVGP]; Fig. 16). Evidence of this glacial ice thinning pertains to the Gállego glacier (SW Pyrenees) and almost disappeared in the Valira glacier (SE Pyrenees). It probably affected both slopes of the Pyrenees. However, the duration of the NLVGP was short on the eastern side of the mountain belt. Most of the nested moraines within the terminal complexes were formed during the latest part of MIS 3 (Fig. 16, STJULIA-2) and progressed during the LGM period of MIS 2 (Fig. 16, LM-1).

Within the terminal complexes incorporating multiple far-flung end moraines (Fig. 17c and d), the oldest end moraine could be beyond the range of luminescence dating (Fig. 17c); this applies to their linked terraces as well (Fig. 17a), like in the Noguera Pallaresa (Fig. 16, SORT-1) and at Cerdanya (Fig. 16, SANAV-1 and SANAV-2).

REFERENCES

Allard, J.L., Hughes, P.D., Woodward, J.C., 2021. Heinrich Stadial aridity forced Mediterranean-wide glacier retreat in the last cold stage. *Nature Geoscience* **14**, 197–205.

Anderson, R.S., Dühnforth, M., Colgan, W., Anderson, L., 2012. Far-flung moraines: exploring the feedback of glacial erosion on the evolution of glacier length. *Geomorphology* **179**, 269–285.

Andrieu V., 1991. *Dynamique du paléoenvironnement de la vallée montagnarde de la Garonne (Pyrénées centrales, France) de la fin des temps glaciaires à l'actuel.* PhD thesis, Université Toulouse 2, Toulouse.

Andrieu, V., Hubschman, J., Jalut, G., Hérail, G., 1988. Chronologie de la déglaciation des Pyrénées françaises. Dynamique de sédimentation et contenu pollinique des paléolacs: application à l'interprétation du retrait glaciaire. *Bulletin de l'Association française pour l'étude du Quaternaire* **25**, 55-67.

Bakalowicz, M., Sorriaux, P., Ford, D.C., 1984. Quaternary glacial events in the Pyrenees from U. series dating of speleothems in the Niaux-Lombrives-Sabart Caves, Ariège, France. *Norsk Geografisk Tidsskrift* **38**, 193–197.

Barr, I. D., Lovell, H., 2014. A review of topographic controls on moraine distribution. *Geomorphology* **226**, 44–64.

Bartolomé M., Sancho C., Benito G., Medialdea A., Calle M., Moreno A., Leunda M., *et al.*, 2021. Effects of glaciation on karst hydrology and

sedimentology during the Last Glacial Cycle: the case of Granito cave, Central Pyrenees (Spain). *Catena* 206, 105252.

Bladé, J.F. 1875. *Études géographiques sur la vallée d'Andorre*. Universelle, París.

Bordonau, J., 1992. *Els complexos glàcio-lacustres relacionats amb el darrer cicle glacial als Pirineus*. Geoforma Ediciones, Logroño, Spain.

Bordonau, J., Pous, J., Queralt, P., Vilaplana, J.M., 1989. Geometría y depósitos de las cubetas lacustres del Pirineo. *Estudios Geológicos* 45, 71–79.

Bordonau, J., Vilaplana, J.M., Fontugne, M., 1993. The glaciolacustrine complex of Llestui (central southern Pyrenees): a key-locality for the chronology of the last glacial cycle in the Pyrenees. *Comptes-Rendus de l'Académie des Sciences, Paris, série II* 316, 807–813.

Bricker, H.M., 2014. The Châtelperronian of the Tambourets (Haute Garonne, France). *PaleoAnthropology* 2014, 1–430.

Buylaert, J.-P., Jai, M., Murray, A.S., Thomsen, K.J., Thiel, C., Sohbati, R., 2012. A robust feldspar luminescence dating method for Middle and Late Pleistocene sediments. *Boreas* 41, 435–451.

Calvet, M., 1994. *Morphogenèse d'une montagne Méditerranéen: Les Pyrénées Orientales*. PhD thesis, Université Paris I–Panthéon–Sorbonne, Paris.

Calvet, M., 1998. Los complejos fluvioglaciares de Cerdanya-Capcir (Pirineos Orientales) y sus enseñanzas. In: Gómez-Ortíz, A., Pérez-Alberti, A. (Eds.), *Las huellas glaciares de las montañas Españolas*. UCS, Santiago de Compostela, pp. 263–291.

Calvet, M., Delmas, M., Gunnell, Y., 2013. Geomorphology of the Pyrenean Orogen. *Postconference Field Excursion P10 from the 8th International Association of Geomorphologists (IAG) Paris*. IAG, Modena, pp. 103–128.

Calvet, M., Delmas, M., Gunnell, Y., Braucher, R., Bourlès, D., 2011a. Le glaciaire du massif du Carlit et les systèmes morainiques terminaux de Cerdagne: éléments de paléogeographie et de chronologie Quaternaire. In: Turu, V., Constante, A. (Eds.), *Simposio de Glaciarismo: El Cuaternario en España y áreas afines, avances en 2011*. AEQUA-Fundació Marcel Chevalier, Andorra la Vella, Andorra, pp. 21–25.

Calvet, M., Delmas, M., Gunnell, Y., Braucher, R., Bourlès, D., 2011b. Recent advances in research on Quaternary glaciations in the Pyrenees. In: Ehlers, J., Gibbard, P.L. (Eds.), *Quaternary Glaciations, Extent and Chronology, a Closer Look*. Part 4. Elsevier, Amsterdam, pp. 127–139.

Camuera, J., Ramos-Román, M.J., Jiménez-Moreno, G., García-Alix, A., Ilvonen, L., Ruha, L., Gil-Romera, G., González-Sampériz, P., Seppä, H., 2022. Past 200 kyr hydroclimate variability in the western Mediterranean and its connection to the African Humid Periods. *Scientific Reports* 12, 1–13.

Catuneanu, O., 2006. *Principles of Sequence Strafigraphy*. Elsevier Science, Amsterdam.

Chevalier, M., 1906. Sur les glaciers Pléistocènes dans les vallées d'Andorre. *Comptes Rendues de l'Académie des Sciences* 41, 662–663.

Chevalier, M., 1907. Les glaciaires Pléistocènes dans les vallées d'Andorre. *Revue Scientifique (revue rose-Sciences et Avenir)* 23, 501–502.

Clapperton, C.M., 1997. Fluctuations of local glaciers 30–8 ka BP: overview. *Quaternary International* 38, 3–6.

Clark, P.U., Dyke, A.S., Shakun, J.D., Carlson, A.E., Clark, J., Wohlfarth, B., Mitrovica, J.X., Hostetler, S.W., McCabe, A.M., 2009. The Last Glacial Maximum. *Science* 325, 710–714.

Copons, R., Bordonau, J., 1996. El registro sedimentario del Cuaternario reciente en el lago Redó d'Aigües Tortes (Pirineo Centrales). *Cuadernos do Laboratorio Xeoloxico de Laxe* 21, 249–260.

Corominas, J., Iglesias, R., Aguasca, A., Mallorquí, J.J., Fàbregas, X., Planas, X., Gili, J.A., 2015. Comparing satellite based and ground based radar interferometry and field observations at the Canillo landslide (Pyrenees). In: Lollino, G., Giordan, D., Crosta, G.B., Corominas, J., Azzam, R., Wasowski, J., Sciarra, N. (Eds.), *Engineering Geology for Society and Territory*. Vol. 2, *Landslide Processes*. Springer, Cham, Switzerland, pp. 333–337.

Daura J., Sanz, M., García, N., Allué, E., Vaquero, M., Fierro, E., Carrión, J.S., et al., 2013. Terrasses de la Riera dels Canyars (Gavà, Barcelona): the landscape of Heinrich Stadial 4 north of the "Ebro frontier" and implications for modern human dispersal into Iberia. *Quaternary Science Reviews* 60, 26–48.

Delmas, M., 2005. La déglaciation dans le massif du Carlit (Pyrénées orientales): approches géomorphologique et géochronologique nouvelles. *Quaternaire,* 16, 45–55.

Delmas M., Braucher R., Gunnell Y., Guillou V., Calvet M., Bourlès D., & ASTER Team, 2015. Constraints on Pleistocene glaciofluvial terrace age and related soil chronosequence features from vertical 10Be profiles in the Ariège River catchment (Pyrenees, France). *Global and Planetary Change* 132, 39–53.

Delmas, M., Calvet, M., Gunnell, M., Braucher, R., Bourlès, D., 2011. Palaeogeography and ¹⁰Be exposure-age chronology of Middle and Late Pleistocene glacier systems in the northern Pyrenees: implications for reconstructing regional palaeoclimates. *Palaeogeography, Palaeoclimatology, Palaeoecology* 305, 109–122.

Delmas, M., Gunnell, Y., Braucher, R., Calvet, M., Bourlès, D., 2008. Exposure age chronology of the last glacial cycle in the eastern Pyrenees. *Quaternary Research* 69, 231–241.

Delmas, M., Gunnell, Y., Calvet, M., Reixach, T., Oliva, M., 2021a. The Pyrenees: glacial landforms prior to the last glacial maximum. In: Palacios, D., Hughes, P., García-Ruiz, J.M., Andres, A. (Eds.), *European Glacial Landscapes: Maximum Extent of Glaciations*. Elsevier, Amsterdam, chap. 40.

Delmas, M., Gunnell, Y., Calvet, M., Reixach, T., Oliva, M., 2021b. The Pyrenees: glacial landforms from the last glacial maximum. In: Palacios, D., Hughes, P., García-Ruiz, J.M., Andres, A. (Eds.), *European Glacial Landscapes: Maximum Extent of Glaciations*. Elsevier, Amsterdam, chap. 59.

Doughty, A. M., Kaplan, M. R., Peltier, C., & Barker, S., 2021. A maximum in global glacier extent during MIS 4. *Quaternary Science Reviews* 261, 106948.

Duller, G.A.T., 2003. Distinguishing quartz and feldspar in single grain luminescence measurements. *Radiation Measurements* 37, 161–165.

Duller, G.A.T., 2004. Luminescence dating of Quaternary sediments: recent advances. *Journal of Quaternary Science* 19, 183–192.

Fernandes, M., Oliva, M., Palma, P., Ruiz-Fernández, J., Lopes, L., 2017. Glacial stages and post-glacial environmental evolution in the Upper Garonne valley, central Pyrenees. *Science of the Total Environment* 584–585:1282–1299.

Fernandes, M., Oliva, M., Vieira, G., Palacios, D., Fernández-Fernández, J.M., Delmas, M., García-Oteyza, J., Schimmelpfennig, I., Ventura, J., 2021. Maximum glacier extent of the Penultimate Glacial Cycle in the Upper Garonne Basin (Pyrenees): new chronological evidence. *Environmental Earth Sciences* 80, 796.

Furdada, G., 1988. *Estudi geomorfològic de la Vall d'Àssua i marge dret de la Ribera de Sort (Pallars Sobirà)*. MSc thesis, Barcelona University, Barcelona.

García-Ruiz, J.M., Martí-Bono, C., Peña-Monné, J.L., Sancho, C., Rhodes, E.J., Valero-Garcés, B., González-Sampériz, P., Constante, A., 2011. El complejo morrénico frontal del valle del Aragón (Pirineos Meridionales). In: Turu, V., Constante, A. (Eds.), *Simposio de Glaciarismo. El Cuaternario en España y áreas afines, avances en 2011*. AEQUA-Fundació Marcel Chevalier, Andorra la Vella, Andorra, pp. 37–43.

García-Ruiz, J.M., Martí-Bono, C., Peña-Monné, J.L., Sancho, C., Rhodes, E.J., Valero-Garcés, B., González-Sampériz, P., Moreno, A., 2013. Glacial and fluvial deposits in the Aragón Valley, central-western Pyrenees: chronology of the Pyrenean late Pleistocene glaciers. *Geografiska Annaler: Series A, Physical Geography* 95, 15–32.

García-Ruíz, J.M., Valero-Garcés, B.L., Martí-Bono, C., González-Sampériz, P., 2003. Asynchroneity of maximum glacier advances in the central Spanish Pyrenees. *Journal of Quaternary Science* 18, 61–72.

Gascón, C., Turu, V., 2011. Pont Trencat: La seqüència sísmica de 1427–1428 a la vall del Valira (Andorra-Alt Urgell, Pirineus Orientals). In: Turu, V., Constante, A. (Eds.), *El Cuaternario en España y Areas Afines (Resúmenes XIII Reunió Nacional de Cuaternario)*. AEQUA-Fundació Marcel Chevalier, Andorra la Vella, Andorra, pp, 97–100.

Giraudi, C., Giaccio, B., 2017. Middle Pleistocene glaciations in the Apennines, Italy: new chronological data and preservation of the glacial record. In: Hughes, P.D., Woodward, J.C. (Eds.), *Quaternary Glaciation in the Mediterranean Mountains*. Geological Society of London Special Publication 433, 161–178.

González-Sampériz, P., Aranbarri, J., Pérez-Sanz, A., Gil-Romera, G., Moreno, A., Leunda, M., Sevilla-Callejo, M., et al., 2017. Environmental

and climate change in the southern Central Pyrenees since the Last Glacial Maximum: a view from the lake records. *Catena* **149**, 668–688.

González-Sampériz, P., Valero-Garcés, B.L., Moreno, A., Jalut G., García-Ruiz, J.M., Martí-Bono C., Delgado-Huertas, A., Navas, A., Otto, T., Dedoubat, J.J., 2006. Climate variability in the Spanish Pyrenees during the last 30,000 yr revealed by the El Portalet sequence. *Quaternary Research* **66**, 38–52.

Guerrero J., Gutiérrez F., García-Ruiz J.M., Carbonel D., Lucha P., Arnold L.J., 2018. Landslide-dam paleolakes in the Central Pyrenees, Upper Gállego River Valley, NE Spain: timing and relationship with deglaciation. *Landslides* **15**, 1975–1989.

Hartevelt, J.J.A., 1970. Geology of the Upper Segre and Valira valleys, Central Pyrenees (Andorra/Spain). *Leidse Geologische Mededelingen* **45**, 167–236.

Hetu, B., Gangloff, P., Courchesne, F., 1992. Un till de déformation du Pléistocene inférieur à la basé de la Formation du Lannemezan (Piémont des Pyrénées Atlantiques, France). *Quaternaire* **3**(2), 53–61

Höbig, N., Weber, M.E., Kehl, M., Weniger, G.-C., Melles, M., Fülöp, R.-H., Vogel, H., Reicherter, K., 2012. Lake Banyoles (northeastern Spain): a Last Glacial to Holocene multi-proxy study with regard to environmental variability and human occupation. *Quaternary International* **274**, 205–218.

Hoey, T.B., 2004. The size of sedimentary particles. In: Evans, D.J.A., Benn D.I. (Eds.), *A Practical Guide to the Study of Glacial Sediments*. Arnold, London, pp. 52–77.

Hughes P. D., Gibbard P. L., Ehlers J., 2013. Timing of glaciation during the last glacial cycle: evaluating the concept of a global "Last Glacial Maximum" (LGM). *Earth-Science Reviews* **125**, 171–198.

Hughes, P.D., Woodward, J.C., van Calsteren, P.C., Thomas, L.E., 2011. The glacial history of the Dinaric Alps, Montenegro. *Quaternary Science Reviews* **30**, 3393–3412.

Hughes, P.D., Woodward, J.C., van Calsteren, P.C., Thomas, L.E., Adamson, K.R., 2010. Pleistocene ice caps on the coastal mountains of the Adriatic Sea. *Quaternary Science Reviews* **29**, 3690–3708.

Huntley, D.J., Baril, M.R., 1997. The K content of the K-feldspars being measured in optical dating or in thermoluminescence dating. *Ancient TL* **15**, 11–13.

[ICGC] Institut Cartogràfic i Geològic de Catalunya, 2006. *Mapa geològic comarcal de Catalunya, Cerdanya. 1:50,000*. Institut Cartogràfic i Geològic de Catalunya, Barcelona.

Jalut, G., Montserrat-Martí, J.M., Fontugne, M., Delibrias, G., Vilaplana, J.M., Julià, R., 1992. Glacial to interglacial vegetation changes in the northern and southern Pyrenees: deglaciation, vegetation cover and chronology. *Quaternary Science Reviews* **11**, 449–480

Jalut, G., Turu, V., 2008. Le dernier cycle glaciaire-interglaciaire dans les Pyrénées: Englacement, Climat, Végétation. In: Canérot, J., Colin, J.-P., Platel, J.P., Bilotte. M. (Eds.), *Pyrénées d'hier et d'aujourd'hui, Biarritz, (France)*. Atlantica, Biarritz, pp. 145–161.

Jalut, G., Turu, V., Dedoubat, J.J., Otto, T., Ezquerra, J., Fontugne, M., Belet, J.M., *et al.*, 2010. Palaeoenvironmental studies in NW Iberia (Cantabrian range): vegetation history and synthetic approach of the last deglaciation phases in the western Mediterranean. *Palaeogeography, Palaeoclimatology, Palaeoecology* **297**, 330–350.

Jiménez-Salas, J.A., de Justo-Alpañes, J.L., 1975. *Geotecnia y cimientos I*. Editorial Rueda, Alcorcón, Madrid.

Kirkbride, M.P., Winkler, S., 2012. Correlation of Late Quaternary moraines: impact of climate variability, glacier response, and chronological resolution. *Quaternary Science Reviews* **46**, 1e29.

Krzyszkowski, D., Zieliński, T., 2002. The Pleistocene end moraine fans: controls on their sedimentation and location. *Sedimentary Geology* **149**, 73–92.

Lewis, C.J., Mcdonald, E.V., Sancho, C., Peña Monné, J.L., Rhodes, E.J., 2009. Climatic implications of correlated Upper Pleistocene and fluvial deposits on the Cinca and Gállego Rivers (NE Spain) based on OSL dating and soil stratigraphy. *Global and Planetary Change* **67**, 141–152.

Lewis, C.J., Sancho, C., Mcdonald, E.V., Peña-Monné, J.L., Pueyo, E.L., Rhodes, E., Calle, M., Soto, R., 2017. Post-tectonic landscape evolution in NE Iberia using staircase terraces: combined effects of uplift and climate. *Geomorphology* **292**, 85–103.

Liu, M., Shen, Y., González-Sampériz, P., Gil-Romera, G., ter Braak, C.J.F., Prentice, I.C., Harrison, S.P., 2021. Holocene climates of the Iberian Peninsula: pollen-based reconstructions of changes in the west-east gradient of temperature and moisture. *Climate of the Past Discussions*. https://doi.org/10.5194/cp-2021-174.

Llobet, S., 1947. *El medio y la vida en Andorra, estudio geográfico*. Instituto Juan Sebastián Elcano-Estación de Estudios Pirenaicos, CSIC, Barcelona.

Luzi, G., Espín-López, P.F., Crosetto, M., Monserrat, O., Barra, A., Gao, Q., 2021. DInSAR deformation measurement using active and passive reflectors. In: *SPIE Remote Sensing Proceedings*. Vol. 11861, *Microwave Remote Sensing: Data Processing and Applications*. https://doi.org/10.1117/12.2600130.

Mardones, M., Jalut, G., 1983. La tourbière de Biscaye (alt. 409 m, Hautes Pyrénées): approche paléoécologique des 45.000 dernières années. *Pollen et Spores* **25**, 163–212

Martinson, D., Pisias, N., Hays, J., Imbrie, J., Moore, T.C. Jr., Shackleton, N., 1987. Age dating and the orbital theory of the Ice Ages: development of a high-resolution 0 to 300,000-year chronostratigraphy. *Quaternary Research* **27**, 1–29.

Martínez-Moreno, J., Mora, R., Casanova, J., 2004. El marco cronométrico de la cueva de l'Estret de Tragó (Os de Balaguer, La Noguera) y la comparación de la vertiente sur de los prepirineos durante el Paleolítico medio. *Saldvie* **4**, 1–16.

Martrat, B., Grimalt, J.O., López-Martínez, C., Cacho, I., Sierro, F.J., Flores, J.A., Zahn, R., Canals, M., Curtis, J.H., Hodell, D.A., 2004. Abrupt temperate changes in the Western Mediterranean over the past 250,000 years. *Science* **306**, 1762–1764.

Mauz, B., Bode, T., Mainz, E., Blanchard, H., Hilger, W., Dikau, R., Zöller, L., 2002. The luminescence dating laboratory at the University of Bonn: equipment and procedures. *Ancient TL* **20**, 53–61.

Mauz, B., Lang, A., 2004a. Removal of the feldspar-derived luminescence component from polymineral fine silt samples for optical dating applications: evaluation of chemical treatment protocols and quality control procedures. *Ancient TL* **22**, 1–8.

Mauz, B., Lang, A., 2004b. The dose rate of beta sources for optical dating applications: a comparison between fine silt and fine sand quartz. *Ancient TL* **22**, 45–48.

McCalpin, J., Corominas, J., 2019. Postglacial deformation history of sackungen on the northern slope of Pic d'Encampadana, Andorra. *Geomorphology* **337**, 134–150.

Mey, P.H.W., 1965. *Geological Map of the Ribagorzana and Baliera Valleys, Central Pyrenees. 1:25,000*. Geological Institute, Leiden University, Leiden.

Montserrat-Martí, J., 1985. *Estudi del Pleistocé superior i de l'Holocé en el rebliment sedimentari de l'Estany de Llauset (Pirineu Ribagorçà)*. Unpublished MSc thesis, Departamento de Geomorfologia i Tectónica, Barcelona University.

Moses C., Robinson D., Barlow, J., 2014. Methods for measuring rock surface weathering and erosion. *Earth-Science Reviews* **135**, 141–161.

Murray, A., Marten, R., Johnston, A., Martin, P., 1987. Analysis for naturally occurring radionuclides at environmental concentrations by gamma spectrometry. *Journal of Radioanalytical and Nuclear Chemistry* **115**, 263–288.

Murray, A.S., Wintle, A.G., 2000. Luminescence dating of quartz using an improved single-aliquot regenerative-dose protocol. *Radiation Measurements* **32**, 57–73.

Murray, A.S., Wintle, A.G., 2003. The single aliquot regenerative dose protocol: potential for improvements in reliability. *Radiation Measurements* **37**, 377–381.

Nussbaum, F., 1934. Die seen der Pyrenäen, Mitt. Nat. Ges., Berne, 184 p. [Translation: Solé, L., 1936. Els llacs dels Pirineus segons Nussbaum, *Butlletí de la Institució Catalana d'Història Natural* **36**(2), 107–115, 1936].

Nussbaum, F., 1956. Observations morphologiques dans la région de la Noguera Pallaresa. *Pirineos* **39–42**, 57–97.

Oliva, M., Palacios, D., Fernández-Fernández, J.M., Rodríguez-Rodríguez, L., García-Ruíz, J.M., Andrés, N., Carrasco, R.M., *et al.*, 2019. Late Quaternary glacial phases in the Iberian Peninsula. *Earth-Science Reviews* **192**, 564–600.

Olley, J.M., Murray, A.S., Roberts, R.G., 1996. The effects of disequilibria in the uranium and thorium decay chains on burial dose rates in fluvial sediments. *Quaternary Science Reviews* **15**, 751–760.

Palacios, D., Gómez-Ortiz, A., Andres, N., Vazquez-Selem, L., Salvador-Franch, F., Oliva M., 2015. Maximum extent of Late Pleistocene glaciers and last deglaciation of La Cerdanya mountains, Southeastern Pyrenees. *Geomorphology* **231**, 116–129.

Pallàs, R., Rodés, A., Braucher, R., Bourlès, D., Delmas, M., Calvet, M., Gunnell, Y., 2010. Small, isolated glacial catchments as priority targets for cosmogenic surface dating of Pleistocene climate fluctuations, SE Pyrenees. *Geology* **38**, 891–894.

Pallàs, R., Rodés, A., Braucher, R., Carcaillet, J., Ortuno, M., Bordonau, J., Bourlès, D., Vilaplana, J.M., Masana, E., Santanach, P., 2006. Late Pleistocene and Holocene glaciation in the Pyrenees: a critical review and new evidence from 10Be exposure ages, south-central Pyrenees. *Quaternary Science Reviews* **25**, 2937–1963.

Panzer, W., 1926. Talentwicklung und eiszeitklima im nordostlichen Spanien. *Abhandlungen der Senckenbergischen Naturforschenden Gesellschaft* **39**, 141–182.

Peña-Monné, J.L., Calvet, M., Turu, V., 2011. Les terrasses fluvials del Segre i afluents principals: Descripció d'afloraments i assaig de correlació. In: Turu, V., Constante, A. (Eds.), *Simposio de Glaciarismo: El Cuaternario en España y áreas afines, avances en 2011*. AEQUA-Fundació Marcel Chevalier, Andorra la Vella, Andorra, pp. 51–55.

Peña-Monné, J.L., Montes, L., Sampietro-Vattuone, M.M., Domingo, R., Medialdea, A., Bartolomé, M., Rubio Fernández, V., *et al.*, 2021. Geomorphological, chronological and paleoenvironmental context of the Neanderthal occupation in the Roca San Miguel site since the penultimate to the last glacial cycle (Arén, Huesca, Spain). *Quaternary Research* **106**, 162–181.

Penck, A., 1884. Die Eiszeit iin den Pyrenäen [The ice age in the Pyrenees]. *Mitteilungen des Vereins für Erdkunde zu Leipzig* **23**, 163–231.

Pérez-Obiol, R., Julià, R., 1994. Climatic change on the Iberian Peninsula recorded in a 30,000-yr pollen record from Lake Banyoles. *Quaternary Research* **41**, 91–98.

Planas, X., Torrebadella, J., 2022. Primeros datos sobre el gran deslizamiento de Vila-Beixalís (Andorra). In: Hürlimann, M., Pinyol, N.M. (Eds.), *X Simposio Nacional sobre Taludes y Laderas Inestables*. CIMNE, Barcelona, pp. 642–653.

Poch, R.M., Simó, I., Boixareda, J., 2013. Benchmark soils on alluvial, fluvial and fluvioal-glacial formations of the upper-Segre valley. *Spanish Journal of Soil Science,* **3**, 78–94.

Prat, M.C., 1980. *Montagnes et vallées d'Andorre, étude géomorphologique.* PhD thesis, Bordeaux III University, Bordeaux.

Railsback, L.B., Gibbard, P.L., Head, M.J., Voarintsoa, N.R.G., Toucanne, S., 2015. An optimized scheme of lettered marine isotope substages for the last 1.0 million years, and the climatostratigraphic nature of isotope stages and substages. *Quaternary Science Reviews* **111**, 94–106.

Rasmussen, S.O., Bigler, M., Blockley, S.P., Blunier, T., Buchardt, S.L., Clausen, H.B., Cvijanovic, I., *et al.*, 2014. A stratigraphic framework for abrupt climatic changes during the Last Glacial period based on three synchronized Greenland ice-core records: refining and extending the INTIMATE event stratigraphy. *Quaternary Science Reviews* **106**, 14–28.

Reimer P., Austin, W., Bard, E., Bayliss, A., Blackwell, P., Bronk Ramsey, C., Butzin, M., *et al.*, 2020. The IntCal20 Northern Hemisphere radiocarbon age calibration curve (0–55 cal kB). *Radiocarbon* **62**, 725–757.

Renault-Miskovsky J., Girard M., 1998. Palynologie des grottes de Montmaurin (Haute-Garonne) et du versant nord pyrénéen. Corrélations interséquentielles du Pléistocène moyen à l'Holocène. *Quaternaire* **9**, 185–201.

Richter, D., Zink, A.J.C., Przegietka, K.R., Cardoso, G.O., Gouveia, M.A., Prudêncio, M.I., 2003. A Source calibrations and blind test results from the new Luminescence Dating Laboratory at the Instituto Tecnologico e Nuclear, Sacavém, Portugal. *Ancient TL* **21**, 43–48.

Rixhon G., 2022. A question of time: historical overview and modern thought on Quaternary dating methods to produce fluvial chronologies. *Quaternaire* **33**, 72–98.

Rodés, A., 2008. *La última deglaciación en los Pirineos: datación de superfícies de exposición mediante* ^{10}Be, *y modelado numérico de paleoglaciares.* PhD thesis, Facultat de Geologia, Universitat de Barcelona, Barcelona.

Rodríguez-Rodríguez, L., Jiménez Sánchez, M., Domínguez-Cuesta, M.J., Rinterknecht, V., Pallas, R., Bourlès, D., 2016. Chronology of glaciations in the Cantabrian Mountains (NW Iberia) during the Last Glacial Cycle based on in situ-produced ^{10}Be. *Quaternary Science Reviews* **138**, 31–48.

Roucoux, K.H., De Abreu, L., Shackleton, N.J., Tzedakis, P.C., 2005. The response of NW Iberian vegetation to North Atlantic climate oscillations during the last 65 kyr. *Quaternary Science Reviews* **24**, 1637–1653.

Salazar-Rincón, A., Mata, M.P., Rico, M.T., Valero-Garcés, B.L., Oliva-Urcia, B., Ibarra, P., Rubio, F.M, Horda Team, 2013. El paleolago de La Larri (Valle de Pineta, Pirineos): significado en el contexto del último máximo glaciar en el Pirineo. *Cuadernos de Investigación Geográfica* **39**, 97–116.

Sancho, C., Arenas, C., Pardo, G., Peña-Monné, J.L., Rhodes, E.J., Bartolomé, M. García-Ruiz, J.M., Martí-Bono, C., 2018. Glaciolacustrine deposits formed in an ice-dammed tributary valley in the South–central Pyrenees: new evidence for late Pleistocene climate. *Sedimentary Geology* **366**, 47–66.

Serrano E., Martínez de Pisón E., González-Trueba J.J., 2011. El complejo lateral de obturación glaciar del barranco de Sia (Alto Gállego, Pirineo Aragonés). In: Turu, V., Constante, A. (Eds.), *Simposio de Glaciarismo: El Cuaternario en España y Áreas afines, avances en 2011*. AEQUA-Fundació Marcel Chevalier, Andorra la Vella, Andorra, pp. 71–76.

Serrat, D., Vilaplana, J.M., 1979. Els dipòsits d'origen glacial de la cubeta de La Massana-Ordino (Andorra): llur significació paleogeogràfica. *Acta Geològica Hispànica* **14**, 433–440.

Serrat, D., Vilaplana, J.M., Martí-Bono, C., 1983. Some depositional models of glaciolacustrine environment in Southern Pyrenees. In: Everson, E.B., Schlüchter, Ch., Rabassa, J. (Eds.), *Tills and Related Deposits.* Balkema,, pp. 132–144.

Sorriaux, P., Delmas, M., Calvet, M., Gunnell, Y., Durand, N., Pons-Branchu, E., 2016. Relations entre karst et glaciaires depuis 450 ka dans la grotte de Niaux-Lombrives-Sabart (Pyrénées ariégeoises). Nouvelles datations U/Th dans la grotte de Niaux. *Karstologia* **67**, 3–16.

Stange, K.M., Van Balen, R., Carcaillet, J., Vandenberghe, J., 2013. Terrace staircase development in the southern Pyrenees foreland: inferences from ^{10}Be terrace exposure ages at the Segre River. *Global and Planetary Change* **101**, 97–112.

Stange, K.M., Van Balen, R.T., Kasse, C., Vandenberghe, J., Carcaillet, J., 2014. Linking morphology across the glaciofluvial interface: a 10Be supported chronology of glacier advances and terrace formation in the Garonne River, northern Pyrenees, France. *Geomorphology* **207**, 71–95.

Thomsen, K.J., Murray, A.S., Jain, M., Bøtter-Jensen, L., 2008. Laboratory fading rates of various luminescence signals from feldspar-rich sediment extracts. *Radiation Measurements* **43**, 1474–1486.

Tomkins, M.D., Dortch, J.M., Hughes, P.D., Huck, J.J., Pallàs, R., Rodés, Á., Allard, J.L., *et al.*, 2021. Moraine crest or slope: an analysis of the effects of boulder position on cosmogenic exposure age. *Earth and Planetary Science Letters* **570**, 117092.

Tomkins, M.D., Dortch, J.M, Hughes, P.D., Huck, J.J., Stimson, A.G., Delmas, M., Calvet, M., Pallàs, R., 2018. Rapid age assessment of glacial landforms in the Pyrenees using Schmidt hammer exposure dating (SHED). *Quaternary Research* **90**, 26–37.

Turu, V., 2000. Aplicación de diferentes técnicas geofísicas y geomecánicas para el diseño de una prospección hidrogeológica de la cubeta de Andorra (Pirineo Oriental): implicaciones paleohidrogeológicas en el contexto glacial andorrano. In: *Actualidad de las técnicas geofísicas aplicadas en hidrogeologia*. ITGE-IGME, Madrid, pp. 203–210.

Turu, V., 2018. High resolution chronostratigraphy from an Iie-dammed palaeo-lake in Andorra: MIS 2 Atlantic and Mediterranean palaeo-climate Inferences over the SE Pyrenees. In: Aliello, G. (Ed.), *New Insights into the Stratigraphic Setting of Paleozoic to Miocene Deposits—Case Studies from the Persian Gulf, Peninsular Malaysia, and South-Eastern Pyrenees.* IntechOpen, London, pp. 63–81.

Turu, V., 1994. Datos para la determinación de la màxima extensión glaciar en los valles de Andorra (Pirineo Central). In: Arnáez-Vadillo, J., García-Ruiz, J.M., Gómez-Villar, A. (Eds.), *Geomorfología en España. Sociedad Española de Geomorfología (SEG).* Vol. 1. Logroño, Spain, pp. 256–273.

Turu, V., Bordonau, J., 1997. El glacialisme de les valls de la Valira del Nord (Principat d'Andorra): Síntesi d'Afloraments. In: *Annals 1995 de l'IEA.* Conselleria d'Educació del Govern d'Andorra, Andorra, pp. 41–104.

Turu, V., Bordonau, J., 2013. Estudio geoquímico de los sedimentos glaciolacustres de la Massana y Ordino (Andorra, Pirineos Orientales): influjo sedimentario entre lagos de obturación yuxtaglaciar e interpretación paleoambiental. In: Baena, R., Fernández, J.J., Guerrero, I. (Eds.), *El Cuaternario Ibérico: Investigación en el s. XXI*. AEQUA-GTPEQ, Sevilla-La Rinconada, Spain, pp. 204–208.

Turu, V., Boulton, G.S., Ros, X., Peña Monné, J.L., Martí Bono, C.E., Bordonau, J., Serrano, E., *et al.*, 2007. Structure des grands bassins glaciaires dans le nord de la Péninsule Ibérique: comparaison entre les vallées d'Andorre (Pyrénées orientales), du Gállego (Pyrénées centrales) et du Trueba (Chaîne Cantabrique). *Quaternaire* **18**, 309–325.

Turu, V., Calvet, M., Bordonau, J., Gunnell, Y., Delmas, M., Vilaplana, J.M., Jalut G., 2017. Did Pyrenean glaciers dance to the beat of global climatic events? Evidence from the Würmian sequence stratigraphy of an ice-dammed palaeolake depocentre in Andorra. In: Hughes, P.D., Woodward, J.C. (Eds.), *Quaternary Glaciation in the Mediterranean Mountains*. Geological Society of London Special Publication 433, 111–136.

Turu, V., Carrasco, M.R., López-Sáez, J.A., Pontevedra-Pombal, X., Pedraza, J., Luelmo-Lautenschlaeger, R., Pérez-Díaz, S., *et al.*, 2021. Palaeoenvironmental changes in the Iberian Central System during the Late-glacial and Holocene as inferred from geochemical data: a case study of the Navamuño depression in Western Spain. *Catena* **207**, 105689.

Turu, V., Carrasco, R.M., Pedraza, J., Ros, X., Ruiz-Zapata, B., Soriano-López, J.M., Mur-Cacuho, E., *et al.*, 2018. Late glacial and postglacial deposits of the Navamuño peatbog (Iberian Central System): Chronology and paleoenvironmental implications. *Quaternary International* **470**, 82–95.

Turu, V., Hirsch, F., Peña-Monné, J.L., Raab, T., Ros, X., Martí-Bono, C., Constante-Orrios, A., 2011. Prospección geofísica y geomecánica de la Ribera de Biescas (Pirineos Centrales): Estructura del relleno sedimentario del fondo del valle y los sedimentos de vertiente. In: Turu, V., Constante, A. (Eds.), *Simposio de Glaciarismo: El Cuaternario en España y áreas afines, avances en 2011*. AEQUA-Fundació Marcel Chevalier, Andorra la Vella, Andorra, pp. 81–91.

Turu, V., Peña-Monné, J.L., 2006. Ensayo de reconstrucción cuaternaria de los valles del Segre y Valira (Andorra–La Seu d'Urgell–Organyà, Pirineos Orientales): morrenas y terrazas fluviales. In: Pérez-Alberti, A., López-Bedoya, J. (Eds.), *Geomorfología y Territorio: IX Reunió Nacional de Geomorfología*. Universidade de Santiago de Compostela, Spain, pp. 129–148.

Turu, V., Planas, X., 2005. Inestabilidad de vertientes en los valles del Valira. Datos y dataciones para el establecimiento de una cronología, posibles causas. Andorra y Alt Urgell (Pirineos Orientales). In: Corominas, J., Romana, M., Hürliman, M., Alonso, J. (Eds.), *Simposio de inestabilidades de vertientes y taludes*. Vol. 3. Universidad Politécnica de Catalunya and Universidad Politécnica de Valencia, Valencia, pp. 795–802.

Ventura, J., Turu, V., 2022. The Noguera Pallaresa glacier evolution (south–central Pyrenees). In: Oliva, M., Palacios, D., Fernández-Fernández, J.M. (Eds.), *Iberia, Land of Glaciers*. Elsevier, Amsterdam, pp. 87–121.

Vidal-Romaní, J.R., Fernández-Mosquera, D., Marti, K., de Brum Ferreira, A., 1999. Nuevos datos para la cronología glaciar pleistocena en el NW de la Península Ibérica. Cadernos Lab. Xeolóxico de Laxe. *Coruña,* **24**, 7–29.

Vidal-Romaní, J.R., Fernández-Mosquera, D., Martin, K., 2015. The glaciation of Serra de Queixa-Invernadoiro and Serra do Geres-Xurés, NW Iberia. A critical review and a cosmogenic nuclide (^{10}Be and ^{21}Ne) chronology. Cadernos Lab. Xeolóxico de Laxe. *Coruña* **38**, 25–44.

Vieira, G., Palacios, D., Andrés, N., Mora, C., Vázquez-Selem, L., Woronko, B., Soncco, C., Úbeda, J., Goyanes, G., 2021. Penultimate glacial cycle glacier extent in the Iberian Peninsula: new evidence from the Serra da Estrela (Central System, Portugal). *Geomorphology* **388**, 107781.

Vilaplana, J.M., 1983a. *Estudi del glacialisme quaternari de les altes valls de la Ribagorça*. PhD thesis, Universitat de Barcelona, Barcelona.

Vilaplana, J.M., 1983b. Quaternary glacial geology of Alta Ribagorça Basin (central southern Pyrenees). *Acta Geològica Hispànica* **18**, 217–233.

Vilaplana, J.M., 1984. *Estudi del glacialisme de les valls de la Valira d'Ordino i d'Arinsal (Andorra)*. Institut d'Estudis Catalans, LXXII S. Ciències, Barcelona.

Vilaplana, J.M., 1985. Les fases glacials del Quaternari superior en el sector nord-oest del Pirineu Andorrà. *Revista d'Investigacions Geològiques* **41**, 67–82.

Vilaplana, J.M., Bordonau, J., 1989. Dynamique sédimentaire lacustre de marge glaciaire: Le paléolac de Llestui (Noguera Ribagorçana-Versant sud des Pyrénées). *Bulletin de l'Association Française pour l'Étude du Quaternaire* **4**, 219–224.

Vilaplana, J.M., Montserrat-Martí, J., Schlüchter, Ch., 1989. Recent progress in Quaternary stratigraphy: the lake Llauset sequence in the Spanish Pyrenees. In: Rose, J., Schlüchter, Ch. (Eds.), *Quaternary Type Sections: Imagination or Reality?* Balkema, Rotterdam, pp. 113–124.

Villa E., Stoll H., Farias P., Adrados L., Edwards R.L., Cheng H., 2013. Age and significance of the Quaternary cemented deposits of the Duje Valley (Picos de Europa, northern Spain). *Quaternary Research* **79**, 1–5.

Walker, M., 2005. *Quaternary Dating Methods*. Wiley, Chichester, UK.

Wintle, A.G., Murray, A.S., 2006. A review of quartz optically stimulated luminescence characteristics and their relevance in single-aliquot regeneration dating protocols. *Radiation Measurements* **41**, 369–391.

Woodward J.C., Hamlin R. H. B., Macklin M. G., Hughes P. D., Lewin J., 2008. Glacial activity and catchment dynamics in northwest Greece: long-term river behaviour and the slackwater sediment record for the last glacial to interglacial transition. *Geomorphology* **101**, 44–67.

Zandvliet, J., 1960. The geology of the Upper Salat and Pallaresa valleys, Central Pyrenees (France/Spain). *Leidse Geologische Mededelingen* **25**, 1–127.

Zwart, H.J., 1979. The geology of the central Pyrenees. *Leidse Geologische Mededelingen* **50**, 1–74.